Chandra News

Issue 19
Spring 2012

Published by the Chandra X-ray Center (CXC)

A Close Nuclear Black Hole Pair in the Spiral Galaxy NGC 3393

G. Fabbiano

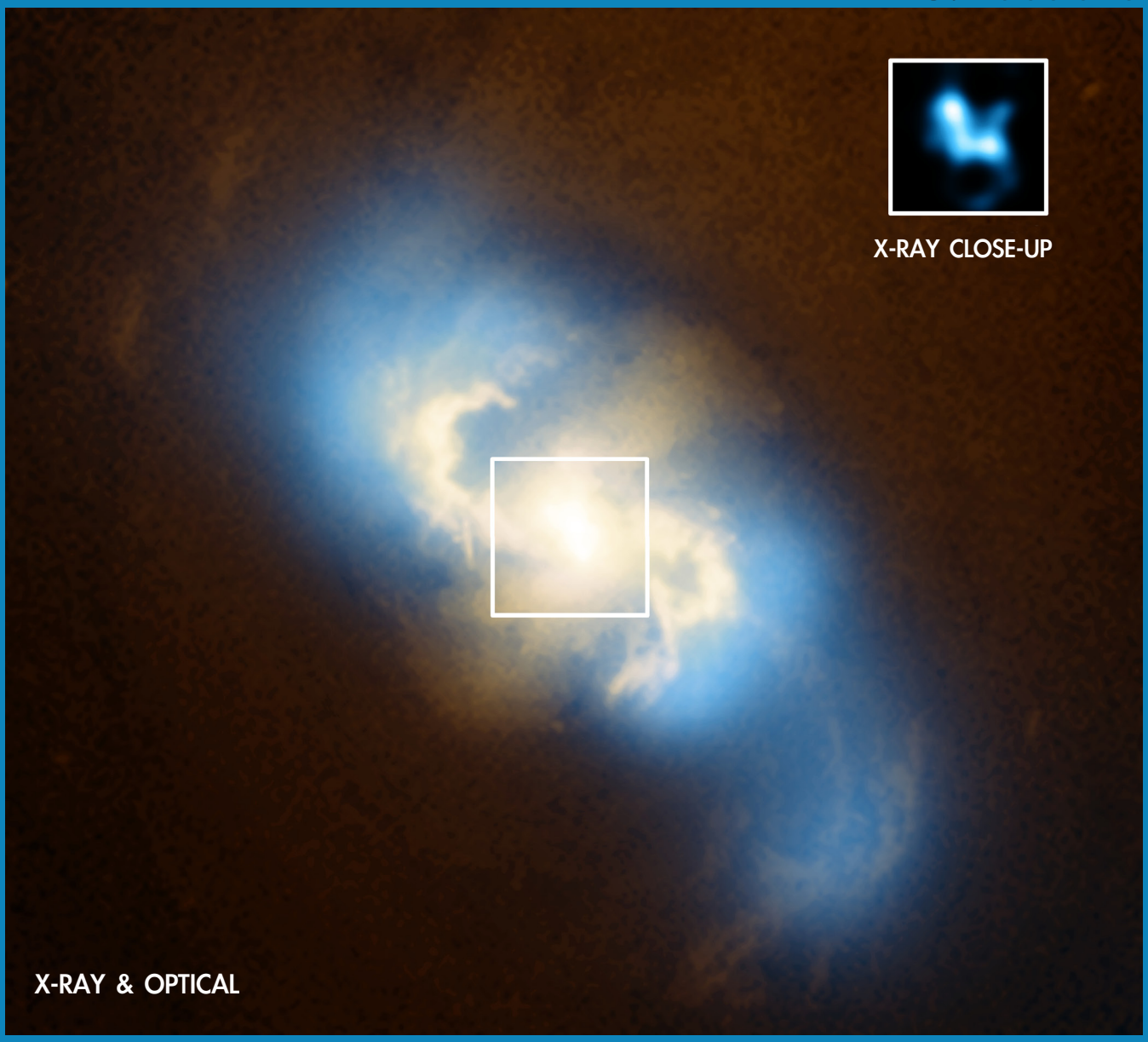

Credit: X-ray: NASA/CXC/SAO/G.Fabbiano et al, Optical: NASA/STScI
Scale: Image is 12.5 arcsec across (about 9,800 light years)
Inset: Image is 1.6 arcsec across (1260 light years)

Contents

The Chandra Newsletter appears once a year and is edited by Paul J. Green, with editorial assistance and layout by Evan Tingle. We welcome contributions from readers.

Comments on the newsletter, or corrections and additions to the hardcopy mailing list should be sent to: chandranews@head.cfa.harvard.edu.

A Close Nuclear Black Hole Pair in the Spiral Galaxy NGC3393

Exploring the inner regions of active galaxies with the highest *Chandra* resolution

G. Fabbiano

The discovery of the M-sigma relation[1], the correlation between the masses of galaxy bulges and those of nuclear massive black holes (MBHs), has suggested that the evolution of galaxies and their MBHs are linked. Both are thought to grow and evolve by merging of smaller galaxy/MBH units pulled together by gravity (see review[2]). During this process, MBHs may also accrete stars and interstellar medium (ISM) from the surrounding merger galaxy, causing the MBH to grow and to "shine" as an active galactic nucleus (AGN). Radiation and winds from the active MBH—AGN feedback—may in turn provide a crucial regulatory mechanism for both galaxy and MBH/AGN growth[3].

The above scenario is consistent with the growing body of multi-wavelength observations, and has been validated by increasingly sophisticated theoretical simulations[4,5]. However, it includes also a big pinch of guesswork. Two open questions stand out: (1) What are the physical parameters of AGN feedback? (2) Can we set strong observational constraints on MBH merger evolution?

Since AGNs are easily detected in X-rays, *Chandra* can play an important role in pursuing these questions at the heart of galaxy evolution.

In this report I will discuss how our project to set observational constraints on AGN feedback with *Chandra* has also led to the discovery of a merging pair of active MBHs, providing a direct observation of later merger evolution.

Chandra observations have shown the entire gamut of nuclear activity from luminous quasars to "silent" or quasi-silent nuclear MBHs[6]. The effect of past AGN activity on the surrounding hot gaseous medium is evident in the large-scale (several to 100s kpc) loops and rings discovered in *Chandra* images of giant elliptical galaxies and clusters[7]. Merger-triggered MBH activity was first imaged with *Chandra* in NGC6240, where a ~2 kpc separation double AGN was discovered, both sources with prominent Fe-Kα lines[8] in their X-ray spectra.

Until recently, these studies were missing the inner (≤100 pc scale) regions of nearby galaxies hosting luminous AGNs, because of the instrumental constraints of ACIS, the most commonly used *Chandra* detector: the imaging resolution limits imposed by the ½ arcsec instrument pixel and the relatively slow ACIS readout resulting in 'pileup' of the strong point-like sources associated with luminous nearby AGNs. However, these inner regions are where we would have the best chance of setting direct observational constraints on the physical parameters of AGN feedback from currently active MBHs, as well as observing active MBHs in a later stage of merging.

In the attempt to investigate the inner circum-nuclear regions of AGNs, post-doc Junfeng Wang, Martin Elvis, Guido Risaliti and I have observed some of these nuclei with the HRC, which although less sensitive and without the energy resolution of ACIS, samples adequately the mirror PSF and is not affected by pileup. We have also acquired deep ACIS data and imaged it with sub-pixel binning (see insert).

Pushing *Chandra*'s Resolution to its Limit: NGC4151

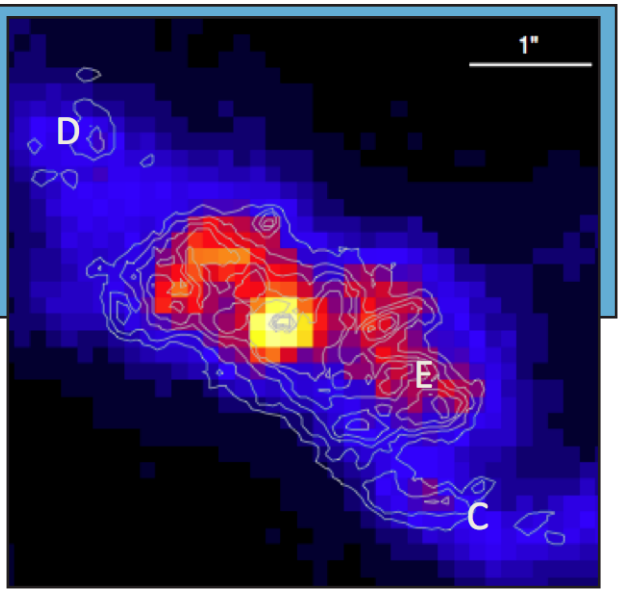

Fig. 1- Deconvolved HRC image[9], compared with [OIII] contours from the HST/FOC (white contours). The letters in the image refer to the regions labeled in the sub-pixel ACIS image shown in Fig. 2.

Our pilot target was NGC4151 (at a distance of 13.3 Mpc). We obtained new deep HRC and ACIS data, which we analyzed in conjunction to the data already available in the *Chandra* archive. The HRC data allows a clean view of the innermost circum-nuclear region (1"~65 pc), which in ACIS is affected by pileup. The HRC instrumental pixel also oversamples the *Chandra* telescope (HRMA) PSF, and therefore the HRC images, although devoid of spectral information, are of a resolution comparable to the limits of the *Chandra* mirrors. The HRC+mirror PSF is well calibrated, allowing image deconvolution to minimize the effect of the PSF wings of the strong nuclear source on the extended circum-nuclear emission[9]. Fig. 1 shows how several features of the deconvolved HRC image of NGC4151 closely

follow features observed in the *Hubble* [OIII] image.

The HRMA's PSF (half-power diameter HPD = 0.6" at E ~ 1.5 keV; see the *Chandra* POG) is under-sampled by the ACIS CCD pixels (0.492" × 0.492"); the ACIS native pixel image of the central region of NGC4151 in the soft energy interval relatively less affected by nuclear pileup, is shown in Fig. 2a. However, the real sampling of the PSF is better than that provided by the ACIS detector pixel, because of the dithering pattern of the *Chandra* telescope. We took advantage of this telescope dithering by using a finer pixel size (0.0625", ~1/8 of the native ACIS pixel size) when extracting the images (see full explanation[10]). This sub-pixel binning approach has been adopted previously in imaging studies of X-ray jets pushing for the highest spatial resolution[11]. The ACIS images with sub-pixel binning (see Fig. 2b) reveal curvy extensions 2" away from the nucleus (labeled as "C" and "D"), which are not discernible in the native pixel soft ACIS image, but are present in both [OIII] and the HRC image.

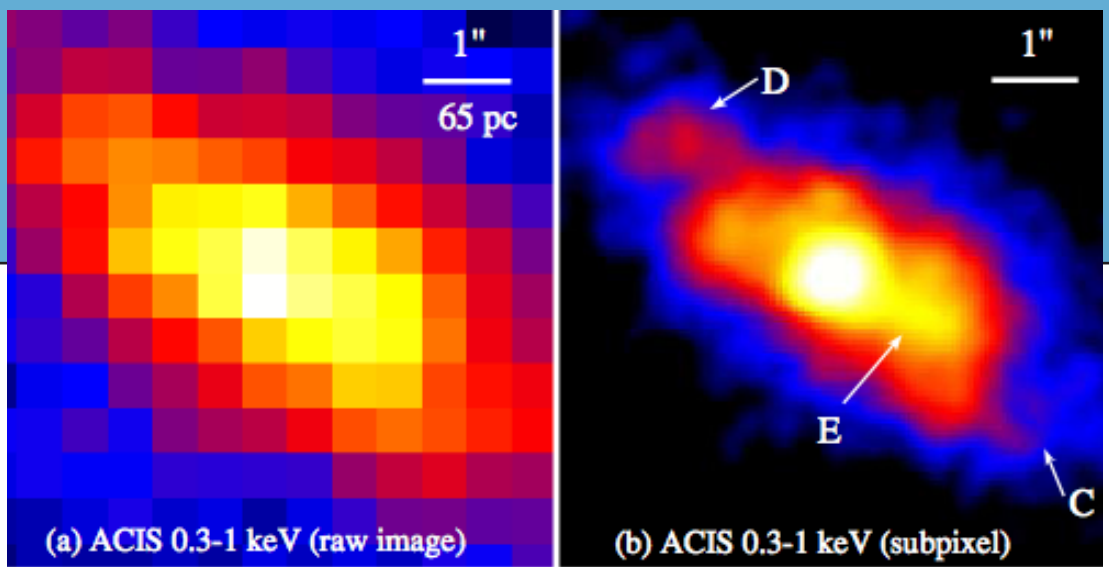

Fig. 2 - a) ACIS image using the native ACIS pixel; b) Same data, sub-pixel binned (1/8 of ACIS pixel), and smoothed with an FWHM = 0".25 Gaussian kernel for better visualization of faint extended features.

By comparing the HRC data with the ACIS sub-pixel image, we demonstrated that we could recover the full resolution of the *Chandra* mirror even in the spatially under-sampled ACIS data. Sub-pixel imaging allows us to expand ultimate high-resolution studies to other active galaxies.

Starting with our pilot study of NGC4151 (PI: Fabbiano), we are now pursuing a program of deep sub-arc-second resolution spatial/spectral studies of the circum-nuclear regions of a sample of nearby AGNs with extended optical emission line regions (CHEERS, PI: J. Wang). We can study details of the circum-nuclear regions down to ~100 pc, spatial scales commensurable with those reached by high-resolution optical and radio telescopes. One of these galaxies is NGC3393, a prominent bulge spiral at a distance of ~50 Mpc, with a highly absorbed (Compton thick[12]) AGN and an extended, spiral like circum-nuclear narrow emission line region (Fig. 3).

NGC3393 had been previously observed with *Chandra* for 30 ks with ACIS[13] to study the Compton thick AGN. This work had reported a nuclear source X-ray spectrum with a featureless continuum and a prominent 6.4 keV Fe-K line. We observed NGC3393 for an additional 70 ks as part of CHEERS. The extended X-ray emission, associated with the optical line emission, is clearly seen in the image (see blue insert in Fig. 3, showing the total screened combined exposure of ~90 ks.) We detected a total of 279±16 counts (3–8 keV) from the nuclear source in the combined exposure, with an ACIS spectrum—also shown in Fig. 3—consistent with that previously reported[13].

Junfeng and I were looking at the combined deep X-ray image using DS9, zooming in to look at the central AGN, when we had a surprise: the hard-band emission (3–8 keV), which should not be affected by softer photo- or shock-ionized circum-nuclear components, did not look point-like. Its spectrum, however, was typical of a Compton-thick AGN (see Fig. 3). The X-ray image, with ¼ pixel binning, is shown in Fig. 4. The X-ray centroid agrees with the emission line central source position (diamond), but the radio position is displaced to the SW, towards the elongation of the X-ray source.

This spatial extension of the hard nuclear emission was puzzling enough to warrant further experimen-

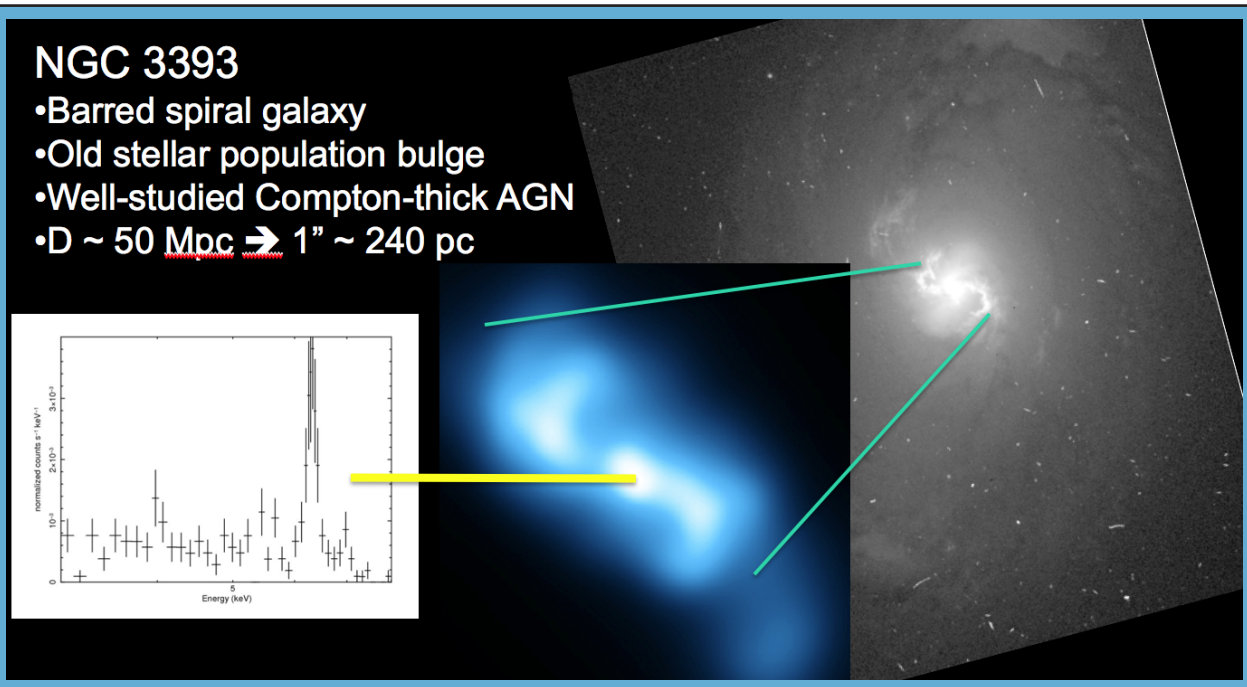

Fig. 3 - HST/WFPC2 F606W image of NGC3393 (gray, background)14 showing the inner ~40" spiral arms, which are also prominent in the [OIII] line, compared with a similar scale ACIS image of the soft X-ray emission (0.3–2 keV), including a total of 90 ks exposure time. The ACIS image is sub-pixel binned (1/4 of the native ACIS pixel, ~0.125") and adaptively smoothed (Wang, J. et al. 2012 in preparation). The nucleus is seen at the center of the X-ray image; the spectrum of the nuclear source shows featureless continuum emission and a prominent Fe-Kα 6.4 keV emission line.

tation. Mindful of the double AGN of NGC6240[8], both with prominent Fe-Kα lines, we decided to derive separate images in the hard continuum (3–6 keV) and in the Fe-K line regions of the spectrum. As can be seen in Fig. 5, a single source, coincident with the optical emission line nucleus, dominates the continuum, while two sources appear in the Fe-K band: one coincident with the optical nucleus, the other closer to the radio position. The two sources are separated by 0.6" in the plane of the sky, corresponding to 150 pc at the distance of NGC3393.

The ACIS spectra of the two sources are shown in Fig. 5; both spectra sport the prominent Fe-Kα lines of Compton-thick AGNs, and each source has X-ray luminosity of a few 10^{42} erg s^{-1}. It appears that NGC3393 contains not one, but two Compton thick obscured active MBHs.

This result is reported in detail in a letter to Nature[15] (*Chandra* press release *http://chandra/photo/2011/n3393/*) and, as discussed there, has clear implications for the galaxy/MBH merger evolution scenario.

The idea of merger evolution was first modeled for the Antennae galaxies and other nearby 'disturbed' galaxies[16]; François Schweizer originally (and controversially) advocated merging of spiral galaxies as a general major formation path for elliptical galaxies[17].

In more recent times, increasingly sophisticated simulations have explored the evolution of galaxies (stars and gaseous components) and their MBH for a range of merging parameters, including major collisions and mergers of similar mass galaxies, minor mergers of different

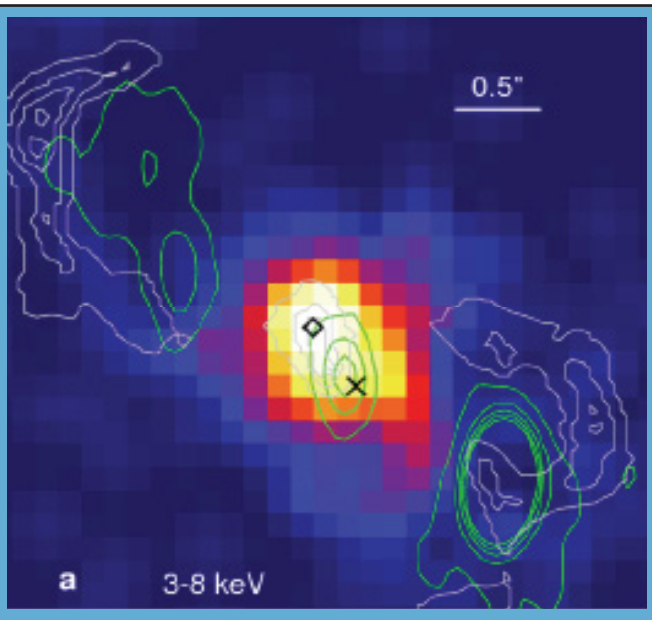

Fig. 4 - 3–8 keV image of the NGC 3393 nuclear region with ¼ subpixel binning, smoothed with a Gaussian of FWHM=0.25". Contours of HST F664N Hα and VLA 8.4 GHz emission are shown in gray and green, respectively (see Fabbiano et al 2011[15] for details and references.)

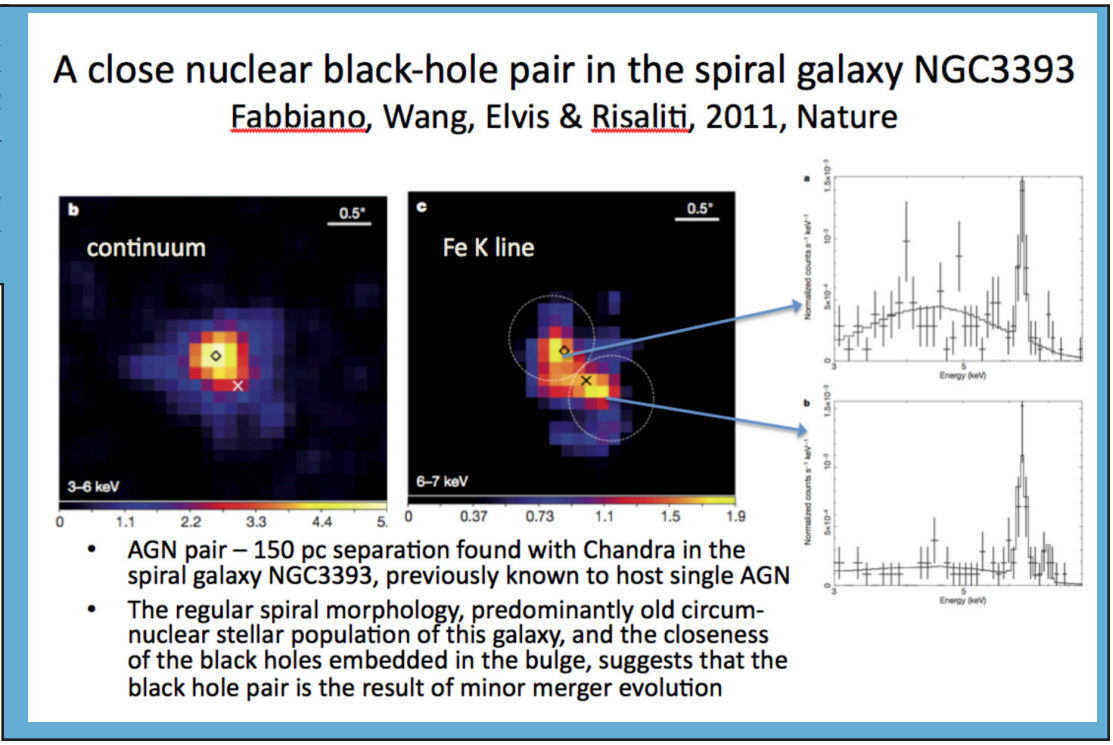

Fig. 5 - b) Continuum image (3–6 keV), with the same processing as in Fig. 4; c) 6–7 keV image, dominated by Fe Kα line emission. The ACIS spectra of the two sources are shown as indicated.

mass galaxies, and looser tidal interactions. While the galaxies interact and merge, the nuclear MBHs are carried along until they are directly interacting with each other. Gravitation drag from stars and even more from gas causes the MBHs to form a close binary, which eventually collapses with emission of gravitational waves[4].

The observational evidence of MBH merging evolution is still rather sparse. Most reported double MBHs are quasar pairs with separation 10 to 100 kpc[18], therefore in the initial stage of their merging interaction. The last stage, with sub-parsec separation leading to MBH collapse and emission of gravitational waves, has been inferred from the spectra and variability of two more quasars[19, 20]. Direct imaging of active MBH pairs in spiral galaxies undergoing a major merger is exemplified by the double AGN of NGC6240[8] with a separation of ~2 kpc, while the double radio nucleus with 7.3 pc separation of the elliptical galaxy 0402+37921 suggests the late evolution of a major merger.

With a separation of 150 pc between the two active MHBs, NGC3393 provides an important and so far unique observational point. The galaxy is a barred spiral, with prominent bulge and grand design arms. Although images show tidal features in the outer region, consistent with gravitational interactions, the morphology is basically regular, suggesting either the later stages of a major merger or a minor merger. The stellar population of the inner bulge does not show any sign of the rejuvenation expected in the case of a major merger for the observed MBH separation, thus arguing for a minor merger. Moreover, in a major merger of similar mass MBHs, the time scale to final collapse at the observed separation of 150 pc would be rather short ~1 Myr, while in the merger of unequal mass galaxies (and MBHs), longer timescales up to 1 Gyr are expected, making the detection of such a system more likely[5].

NGC3393 is the first reported double AGN with ~100 pc scale separation in a spiral galaxy. Simulations suggest that the detection of such a close AGN pair should be a relatively rare event[22, 23], so we may have just been lucky. However, I believe it's healthy as an observer to keep an open mind, and not to be unduly influenced by theory. The observational constraints are still rather loose: NGC3393 is only one observational point. Even another detection in a well-defined sample would provide important information. One thing we have learnt from NGC3393 is that normal looking large bulge galaxies, not just clearly disturbed mergers, may be a good hunting ground for closely interacting merging active MBHs. We intend to continue pursuing this hunt with *Chandra* in the future.

References

[1]Magorrian, J., Tremaine, S., Richstone, D., Bender, R., Bower, G., Dressler, A., Faber, S. M., Gebhardt, K., Green, R., Grillmair, C., Kormendy, J., & Lauer, T. (1998). AJ 115:2285-2305.
[2]Colpi, M. & Dotti, M. (2009). ArXiv:0906.4339.
[3]Di Matteo, T., Springel, V., & Hernquist, L. (2005). Nature

433:604-607.
[4]Mayer, L., Kazantzidis, S., Madau, P., Colpi, M., Quinn, T. & Wadsley, J. (2007). Science 316:1874-1877.
[5]Callegari, S., Kazantzidis, S., Mayer, L., Colpi, M., Bellovary, J. M., Quinn, T. & Wadsley, J. (2011). ApJ 729:85.
[6]Pellegrini, S. (2005). ApJ 624:155-161.
[7]Fabian, A. C., et al. (2011). MNRAS, 418, 2154-2164 .
[8]Komossa, S., Burwitz, V., Hasinger, G., Predehl, P., Kaastra, J. S. & Ikebe, Y. (2003). ApJ 582:L15-L19.
[9]Wang, J., Fabbiano, G., Karovska, M., Elvis, M., Risaliti, G., Zezas, A. & Mundell, C. G. (2009). ApJ 704:1195.
[10]Wang, J., Fabbiano, G., Risaliti, G., Elvis, M., Karovska, M., Zezas, A., Mundell, C. G., Dumas, G. & Schinnerer, E. (2011). ApJ 729:75.
[11]Harris, D. E., Mossman, A. E., & Walker, R. C. (2004). ApJ 615:161.
[12]Maiolino, R., Salvati, M., Bassani, L., Dadina, M., della Ceca, R., Matt, G., Risaliti, G. & Zamorani, G. (1998). A&A 338:781-794.
[13]Levenson, N. A., Heckman, T. M., Krolik, J. H., Weaver, K. A. & Życki, P. T. (2006). ApJ 648:111-127.
[14]Malkan, M. A., Gorjian, V. &Tam, R. (1998). ApJ 117:25.
[15]Fabbiano, G., Wang, J., Elvis, M. & Risaliti, G. (2011). Nature 477:431.
[16]Toomre, A. & Toomre, J. (1972). ApJ 178:623-666.
[17]Schweizer, F. (1982). ApJ 252:455-460.
[18]Green, P. J., Myers, Adam D., Barkhouse, W. A., Mulchaey, J. S., Bennert, V. N., Cox, T. J. & Aldcroft, T. L. (2010). ApJ 710: 1578-1588.
[19]Boroson, T. A. & Lauer, T. R. (2009). Nature, 458:53-55.
[20]Valtonen, M. J., Lehto, H. J., Nilsson, K., Heidt, J., Takalo, L. O., Sillanpää, A., Villforth, C., Kidger, M., Poyner, G., Pursimo, T., et al. (2008). Nature 452:851-853.
[21] Rodriguez, C., Taylor, G. B., Zavala, R. T., Peck, A. B., Pollack, L. K. & Romani, R. W. (2006). ApJ 646: 49-60.
[22]Blecha, L., Loeb A. & Narayan, R. (2012). ArXiv:1201.1904.
[23]Van Wassenhove, S., Volonteri, M., Mayer, L., Dotti, M., Bellovary, J., & Callegari, S. (2011). arXiv:1111.0223.

Project Scientist's Report

Martin Weisskopf

"The marvel of *Chandra* exceeding its nominal operational life continues." With these words, we began last year's report. We hope to repeat them for many years to come. The Observatory is now in its 13th year of successful operation, and the call for the Cycle 14 proposals has been issued.

The *Chandra* Team has submitted its proposals to the NASA 2012 Senior Review of Operating Missions. The submission included two proposals: one for the *Chandra* mission and the other for Education and Public Outreach. Oral presentations to the Senior Review Committee are scheduled for February 29.

The *Chandra* X-ray Observatory is unique in its capability for sub-arcsecond X-ray imaging, which is essential to the science goals of many key X-ray and multi-wavelength astrophysical investigations. The Observatory continues to operate with only minor incremental changes in performance, due primarily to the gradual accumulation of molecular contamination on the ACIS filters and to slow degradation of the spacecraft's thermal insulation. The former affects the detection of low-energy x-rays with ACIS. The latter impacts observing scheduling and strategies to ensure continued operation of the Observatory in a safe thermal environment.

In late 2012 January, *Chandra* experienced the strongest solar proton events since the previous solar maximum. The consequence of such radiation storms is that the Observatory must suspend science operations until the high flux of damaging protons has subsided. In preparation for the impending solar maximum, the *Chandra* Team has made some innovations to respond more robustly to solar proton events. These include use of the HRC anti-coincidence shield rate and of the ACIS threshold crossings as onboard radiation monitors, as well as the implementation of a "Science-Only Safing Action" (SOSA). The SOSA splits the (nominally) weekly command loads into vehicle and science-observation commands, which now allows the spacecraft to continue scheduled maneuvers and other vehicle activities even when the science load has stopped—e.g., to protect the instruments from radiation damage.

A major highlight this past year was the introduction of a new proposal category—X-ray Visionary Projects (XVP)—to address key astrophysical questions that require 1–6 Ms of observing time. The last peer review awarded time for 4 XVPs: "A *Chandra* Legacy Project to Resolve the Accretion Flow of Gas Captured by a Supermassive Black Hole" (1 Ms); "Cosmology and Cluster Evolution from the 80 Most Massive Clusters in 2000 deg^2 from the South Pole Telescope Survey" (2 Ms); "*Chandra* Exploration of the Cosmic Melting Pot in the Virialization Region of a Rich Galaxy Cluster" (2 Ms); "*Chandra* HETG Ultra-deep Gratings Spectroscopy of Sgr A*" (3 Ms). Overall, the Cycle 13 Peer Review approved 199 of 664 submitted research proposals, which had requested 142 Ms of observing time, a factor-of-5.4 oversubscription of the available 27 Ms. (See Belinda Wilkes' article for details.)

Project Manager's Report

Roger Brissenden

***Chandra* marked over twelve years of successful mis**sion operations with continued excellent operational and scientific performance. Telescope time remained in high demand, with significant oversubscription in the Cycle 13 peer review held in June. In the Fall the observing program transitioned from Cycle 12 to Cycle 13. We released the Call for Proposals for Cycle 14 in December, and look forward to the Cycle 14 peer review in June 2012.

The team worked hard to prepare for NASA's 2012 Senior Review of operating missions. The CXC submitted our proposal in January 2012 (with the Education and Public Outreach proposal submitted separately in December, 2011), and will participate in an oral presentation to the Senior Review committee at the end of February 2012.

The CXC conducted several workshops and symposia during 2011. We celebrated *Chandra*'s 12th anniversary with the symposium "12 Years of Science with *Chandra*," part of the American Astronomical Society meeting held in Boston in May. In July we conducted the workshop "Structure of Clusters and Groups of Galaxies in the *Chandra* Era," and in August held the 2011 5-day X-ray Astronomy School, followed by a workshop for users of the CXC's CIAO data analysis software system. As part of the CXC's regular reviews and consultations with outside organizations, NASA reviewed the CXC's operations in March and September, and the *Chandra* Users' Committee met at the CXC in October.

The CXC mission planning staff continued to maximize observing efficiency in spite of temperature constraints on spacecraft pointing. Competing thermal constraints continue to require that some longer observations be split into multiple short duration segments, to allow the spacecraft to cool at preferred attitudes. The total time available for observing has been increasing gradually over the past few years as *Chandra*'s orbit evolves and the spacecraft spends less time in Earth's radiation belts. The overall observing efficiency during 2011 was 75%, compared with 74% in 2010 and an average of 68% over the mission. In the next several years we expect potential
observing time to increase slightly, but actual observing to be limited by radiation due to increasing solar activity.

Operational highlights over the past year included five approved requests to observe targets of opportunity that required the mission planning and flight teams to interrupt and revise on-board command loads. After several years of very low solar radiation, the sun has become more active, causing the team to interrupt *Chandra* observing three times during the year to protect the instruments from solar particles. *Chandra* passed through the 2011 summer and winter eclipse seasons, as well as a brief lunar eclipse in June, with nominal power and thermal performance.

Chandra's first full safe mode event in over 11 years—ultimately shown to have no hardware cause—occurred in July. On-board software detected an anomalous change in the spacecraft's angular momentum, triggering an autonomous transition to safe mode and a resulting swap to redundant hardware. The swap went flawlessly and all of the redundant systems performed as expected. The CXC's flight and science staff changed immediately to 24-hour operations and scheduled extra telemetry contacts with the spacecraft. Analysis of spacecraft data and orbital dynamics revealed that the safe mode transition resulted from a complex interaction of gravity-gradient torques, commanding in the science loads, and flight software timing. No hardware failures were involved and no harm was caused to the Observatory. The staff returned *Chandra* to nominal observing five days after the anomaly occurred, with a loss of 370 ks of observing time. The event demonstrated the training, effectiveness and seamless cooperation of all elements of the *Chandra* X-ray Observatory team.

In October, the spacecraft transitioned to normal sun mode when an electronic circuit reset, believed to be due to a single event upset, in which radiation or ions interrupt a component in the on-board electronics. The operations teams returned the spacecraft to normal status within two days with no adverse consequences, but the loss of 154 ks of observing time.

As part of an on-going risk reduction program, the CXC flight team identified a method to improve *Chandra*'s response to high radiation as the sun becomes more active. The new process maintains the science instruments in a radiation-safe condition while allowing controllers to continue spacecraft management activities such as eclipse response, attitude control, and thermal and momentum management. The new safing approach reduces risk to the spacecraft and minimizes the time and effort required to resume observations after a high radiation event. Following software development and extensive ground testing, the new method was fully implemented on 1 December 2011 and first came into action during a radiation safing in January, 2012.

Both focal plane instruments, the Advanced CCD Imaging Spectrometer and the High Resolution Camera, have continued to operate well and have had no significant problems. ACIS, along with the overall spacecraft, has continued to warm gradually.

All systems at the *Chandra* Operations Control Center continued to perform well in supporting flight operations.

Chandra data processing and distribution to observers continued smoothly, with the average time from observation to delivery of data averaging roughly 30 hours. The *Chandra* archive holdings grew by 0.5 TB to 8.8 TB and now contain 32.7 million files. *Chandra* Source Catalog data products represent 1.8 TB of the archive.

The Data System team released software updates to support the submission deadline for Cycle 13 observations proposals (March 2011), the Cycle 13 Peer Review (June) and the Cycle 14 Call for Proposals (December 2011). Software upgrades supported the multi-cycle observing proposals that were solicited beginning in Cycle 13.

In addition, several enhancements to instrument algorithms have been incorporated into standard data processing and also released in CIAO 4.4 (December), including a new ACIS afterglow/hot pixel determination tool. Work is progressing on a new version of the *Chandra* Source Catalog (CSC) that will increase the number of detected X-ray sources. The new CSC version will extend the catalog to fainter limits by combining multiple observations and by using new algorithms to allow point sources as faint as ~5 counts to be detected on-axis, resulting in a ~2.5 times increase in the number of X-ray sources included in the catalog.

The CXC Education and Public Outreach (EPO) group in 2011 created 15 science press releases, a press release posting and 12 image releases, and produced 22 60 second High Definition podcasts on astrophysics and *Chandra* results. Two of the group's animated videos earned platinum-level Pixie awards from the American Pixel Academy. CXC staff created 75 blog entries, and initiated live tweets from such venues as the AAS meeting, science fairs and the NASA press conference.

EPO personnel presented 26 workshops at conferences and clinics sponsored by the National Science Teacher Association, National Science Olympiad, American Association of Physics Teachers, and the Astronomy Society of the Pacific. EPO staff presented an invited talk on public science at the October conference Communicating Astronomy with the Public, sponsored by the International Astronomical Union.

The EPO group was awarded a grant to support NASA's Year of the Solar System initiative by developing the exhibit From Earth to the Solar System, modeled on the EPO-created exhibit From Earth to the Universe (FETTU). The Braille panels developed for FETTU were donated to the National Federation for the Blind for permanent exhibit at its Jernigan Institute.

We look forward to a new year of continued smooth operations and exciting science results. Please join us for the workshop "X-ray Binaries, 50 Years Since the Discovery of Sco X-1", to be held in Boston July 10–12, 2012.

Important Dates for *Chandra*

Cycle 14 Peer Review: June 25–29, 2012

Workshop: July 10–12, 2012
50 Years of X-ray Binaries

Cycle 13 Cost Proposals Due: Fall 2012

Users' Committee Meeting: October, 2012

Einstein Fellows Symposium: Fall 2012

Cycle 14 Start: December, 2012

Cycle 15 Call for Proposals: December, 2012

ACIS Update

Paul Plucinsky, Royce Buehler, Nancy Adams-Wolk, & Gregg Germain

The ACIS instrument continued to perform well over the past year with no anomalies or unexpected degradations. The charge-transfer inefficiency (CTI) of the FI and BI CCDs is increasing at the expected rate. The contamination layer continues to accumulate on the ACIS optical-blocking filter. Recent data indicate that the contaminant may be increasing in thickness faster than the current model predicts, especially around the edges of the filter which are colder than the center of the filter. The CXC calibration group is analyzing the data and may produce an updated contaminant model in the coming year.

The control of the ACIS focal plane (FP) temperature continues to be a major focus of the ACIS Operations Team. As the *Chandra* thermal environment continues to evolve over the mission, some of the components in the Science Instrument Module (SIM) close to ACIS have been reaching higher temperatures, making it more difficult to maintain the desired operating temperature of -119.7° C at

the focal plane. In previous years, a heater on the ACIS Detector Housing (DH) and a heater on the SIM were turned off to provide more margin for the ACIS FP temperature. At this point in the mission, there are two effects that produce excursions in the FP temperature, both related to the attitude of the satellite. First the Earth can be in the FOV of the ACIS radiator (which provides cooling for the FP and DH). Second, for pitch angles larger than 130 degrees, the Sun illuminates the shade for the ACIS radiator and the rear surfaces of the SIM surrounding the ACIS DH. Reducing the number of operational CCDs reduces the power dissipation in the FP, thereby resulting in a lower FP temperature.

Starting in Cycle 13, GOs were encouraged to request 5 CCDs for their observations to keep the FP and the electronics cooler, if their science objectives could be met with 5 CCDs. Starting in Cycle 14, GOs will not be allowed to specify "Y" for 6 CCDs in the RPS forms when they submit their proposal. If a GO requires 6 CCDs for their observation, they are to specify 5 CCDs as "Y" and one CCD as "OPT1" at the time of proposal submission. If the proposal is selected, the GO may work with their User Uplink Support Scientist and change the "OPT1" to a "Y" if the sixth CCD is required. GOs should be aware that requesting 6 CCDs increases the likelihood of a warm FP temperature and/or may increase the complexity of scheduling the observation. GOs should review the updated material in the Proposers' Guide on selecting CCDs for their observations and on this web page: *http://cxc.cfa.harvard.edu/acis/optional_CCDs/optional_CCDs.html*

The control of the ACIS electronics temperatures has also been a concern for the ACIS Operations Team. ACIS has three main electronics boxes, the Power Supply and Mechanisms Controller (PSMC), the Digital Processing Assembly (DPA), and the Detector Electronics Assembly (DEA). The PSMC reaches its highest temperatures when the satellite is in a "forward Sun" configuration, pitch angles between 45–60 degrees (*Chandra* cannot point within 45 degrees of the Sun). Since 2006, the *Chandra* FOT has been using the optional CCDs information provided by GOs to turn off optional CCDs if thermal conditions require. As a result of the changing thermal environment, the DEA and DPA are reaching higher temperatures in tail-Sun orientations (pitch angles larger than 130 degrees). The recommendation in the previous paragraph to use only 5 CCDs if the science objectives can be met with 5 CCDs, will also reduce the temperature of the DEA and DPA in addition to the temperature of the FP. Starting in Cycle 14, the *Chandra* FOT will be using the optional CCDs information to turn off optional CCDs if either the DEA or DPA approach their temperature limits.

HRC Update

Ralph Kraft and Junfeng Wang

Another year has passed and the HRC continues to operate normally. There have been no significant changes or performance anomalies since the last *Chandra* newsletter. However, as described in detail in Jeremy Drake's article on LETG, the CXC calibration team felt that the gain loss, and therefore quantum efficiency loss (40% or more at some locations), due to charge extraction in the wing plates of the HRC-S was sufficiently large that it would start to impact science observations. This slow decay in instrument gain and QE is a well-known effect in microchannel plate (MCP) detectors, and the HRC was designed with the capability to raise the high voltage to recover the gain.

Accordingly, a plan was developed (principally by Mike Juda and the CXC Calibration team with the support of the HRC instrument team) to evaluate the effect of a progressive increase of the high voltage on both the top and bottom MCPs and determine how much of the lost QE in the wing plates could be recovered by a small increase to the HV. This plan was implemented during a realtime contact on the morning of January 9th, 2012. A Command Action Procedure was developed in which the HV on the HRC-S would be raised above the nominal operating voltage one digital step at a time while observing HZ 43 with the LETG inserted (30 cts s^{-1} in the dispersed spectrum in the wing plates). The voltages were to be raised by 3 steps on each plate, or roughly 50 volts above the nominal 1250 V operating voltage. Roughly 10 minutes of data would be taken at each voltage step so that the progressive change could be evaluated. This would occur during a realtime telemetry contact so that the instrument team could continuously monitor the performance and safety of the instrument. The HV would be returned to its nominal operating setting at the end of the experiment.

At the time of writing this article, we are just receiving the processed data from this experiment. Quick look realtime analysis at the OCC showed that the detector performed as expected at the higher voltages and that there were no problems with increased background or hot spots in the detector during the operation. The HRC was returned to its default configuration and seen to be operating normally at the end of experiment. Preliminary analysis of the processed data from the first few voltage steps shows that the source rate did increase by roughly 10% per voltage step. A more careful analysis is underway by both the CXC Cal and HRC instrument teams to evaluate the effect on gain and QE. If the data shows that we recover most or all

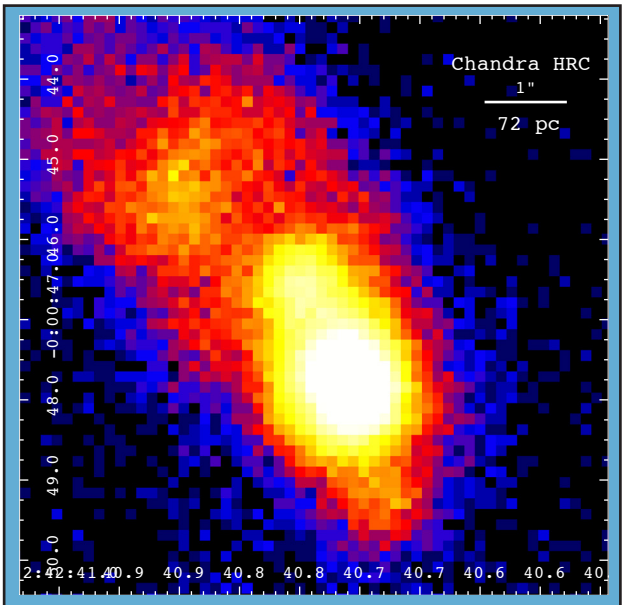

Fig. 1. - The ~7" x 7" (500 pc across) HRC image of NGC 1068 obtained in ObsID 12705.

of the QE by increasing the gain, the HV on the HRC-S may be permanently increased. A similar procedure eventually may be needed to increase the voltage on the HRC-I plates, but charge extraction monitoring shows a smaller gain loss in the imager to date.

The HRC continues to be used for a wide range of scientific investigations. Junfeng Wang, Margarita Karovska, Pepi Fabbiano and collaborators used the HRC plus image deconvolution to resolve structures on sub-arcsecond scales near the nucleus in the Seyfert 2 AGN NGC 1068. As described in detail in Pepi Fabbiano's contribution, the HRC is being used in a number of investigations to resolve sub-arcsecond structure in the vicinity of bright AGN. The HRC is particularly useful in these observations because the pixel scale closely matches the telescope PSF and the HRC does not suffer from pileup due to the bright AGN.

Motivated by the HRC discovery of the jet-gas cloud interaction in the nuclear region of NGC 4151 (Wang et al. 2009ApJ 704,1195), the first HRC image of the prototype Compton-thick Seyfert 2 galaxy NGC 1068 (1"~72 pc) was recently obtained (Fig. 1, 40 ks exposure, PI: Fabbiano). The HRC image clearly resolves the subarcsecond structures associated with the narrow line region clouds, which cannot be studied in previous ACIS imaging observations due to the overwhelming pileup of the bright X-ray nucleus. The PSF-deconvolved HRC image using the EMC2 algorithm (see Karovska et al. 2005, ApJL 623, 137 and references therein) provides an unprecedented morphological comparison between the X-ray emission and the radio jet in the innermost 100 pc of this galaxy (Fig. 2), allowing us to study in detail the disruption of the collimated inner radio jet (Wang, Fabbiano, Karovska et al. 2012 in prep.). The overlay shows X-ray emission "blobs" at the locations where the radio jet (green contours) changes direction and where the highly collimated jet terminates, implying possible interactions with the gas clouds.

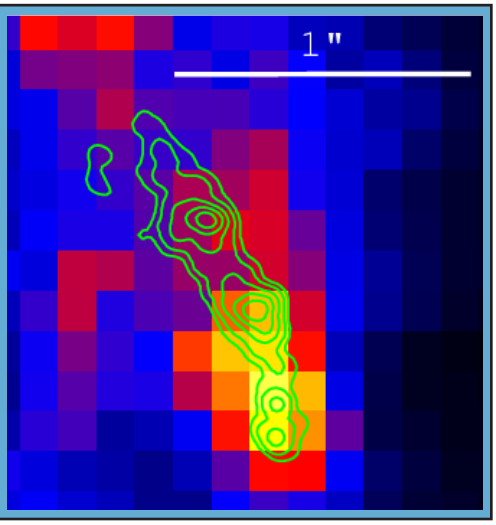

Fig. 2 - X-ray emission structure in the innermost 100 pc region of NGC 1068, revealed by the HRC image with EMC2 deconvolution. Superposed are contours from 5 GHz MERLIN radio image (courtesy of J. Gallimore).

HETGS Calibration Update

Herman Marshall

A new set of HETGS efficiencies was released as part of CalDB v4.4.7, which should reduce systematic differences between the HEG and MEG fluxes as well as improve overall model fits. Here, I'll summarize the steps that went into the release and what is in store for the next update. Details will be available at the HETGS calibration web site *http://space.mit.edu/ASC/calib/hetgcal.html* and will be presented at the next meeting of the International Astronomical Consortium for High Energy Calibration (IACHEC) in March (see *http://web.mit.edu/iachec/meetings/index.html*). First, data were selected from the TGCat online catalog of HETGS spectra. See *http://tgcat.mit.edu* to obtain the data used here. I started with sources of all sorts but relied most on those with simple continua. Next, the +1 and −1 fluxes were compared for both MEG and HEG in order to verify that 1) the chip QEs are consistent and 2) that contamination correction of one grating "arm" is consistent with the other (because there is a spatial variation to the contaminant's thickness). All fluxes came out to be consistent to within 1% on average except near 0.5 keV, where the two sides differ by 3–5% but generally within the statistical uncertainties.

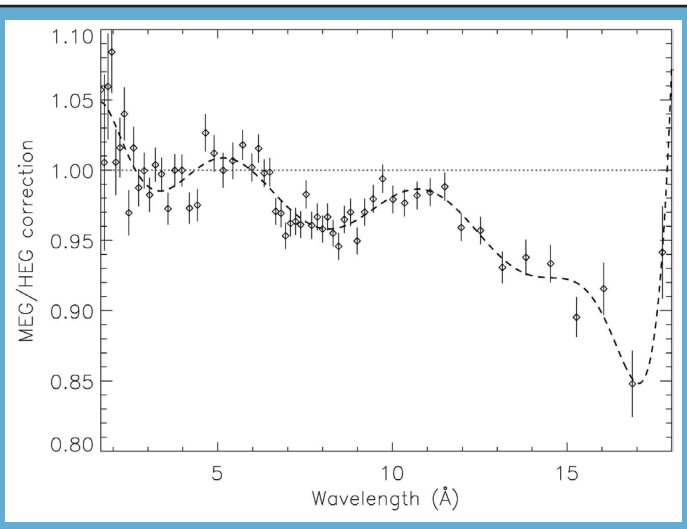

Fig. 1 - The ratio of the MEG and HEG fluxes as a function of wavelength, binned to have 1% uncertainties or bin widths less than 5% of the central wavelength. The sense of the correction is that the values shown should be applied to the MEG efficiencies to bring MEG fluxes into agreement with those derived from HEG data. The dashed line is a 9th order polynomial fit to the data.

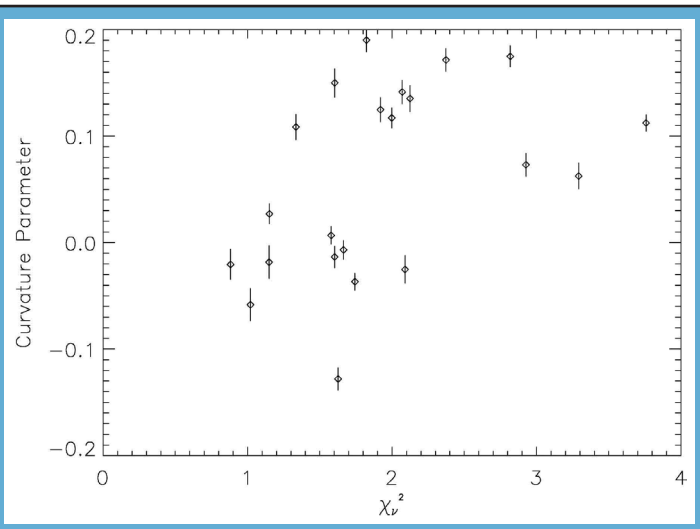

Fig. 2 (above)- The curvature parameter β, as a function of reduced χ^2 for fits to HETGS spectra of AGN. See Eq. 1 for the model, which defines β.

Fig. 3 (below)- The average residuals for curved power law fits to the HETGS data for 8 BL Lac objects. For most of the HETGS range, the systematic deviations are not significant or are less than 3%. Deviations of 5–10% near 6 keV and 0.7 keV will be investigated further.

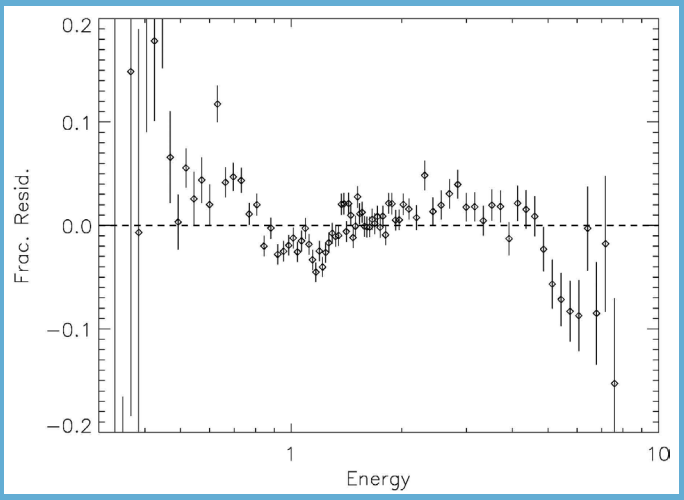

Fig. 1 shows the ratio of the MEG and HEG fluxes as a function of wavelength, binned to have 1% uncertainties so that small systematic errors may be found and corrected. Because the polynomial fit can correct only the ratio of the MEG and HEG efficiencies, I allocated the correction to either the HEG or MEG efficiencies: longer than a specified wavelength, all corrections are applied to the HEG, while for shorter wavelengths, the MEG is corrected. The simple reasoning behind the choice is that it was somewhat easier to determine HEG efficiencies on the ground at high energies due to the higher resolution while harder to measure them at low energies due to significantly lower effective area. Furthermore, the HEG part of the HETGS dominates observations at high energy while the MEG part dominates at low energy, so a "least harm" dictum suggests applying less correction where a grating part dominates. I tried several possible cross-over wavelengths and found that 10 Å minimized the reduced χ^2 in BL Lac fits (see below).

For about 20 observations of AGN, I applied the new corrections to the HETGS spectra and fit them to a simple logarithmic parabola model with four parameters:

Eq. 1 $$n_E = A\, e^{-N_H \sigma(E)} E^{-\Gamma+\beta \log E}$$

where N_H was fixed for each AGN to an estimate based on 21 cm data (the results are robust against the exact choice), and the overall model is a power law with a curvature term, β. The model is the same as that used for BL Lac objects by Perlman et al.[1]. The curvature term is negative for spectra that are convex upward and positive for those with soft or hard excesses. Fig. 2 shows that the quality of the fit is related to the value of β: better fits are obtained for negative curvature. The fits with positive curvature were predominantly radio-loud AGN with emission lines, indicating that these spectra are actually more complex than a simply curving model provides. For the remaining analysis, the sources with $\beta < 0.3$ were chosen; these were the BL Lac objects PKS 2155-304 and 1H 1426-428. The curvature values are similar to those found for other BL Lac objects[1].

The spectral residuals for the BL Lac objects were

combined in order to see if there were significant remaining residuals. Fig 3 shows the result. While there are possible systematic errors of up to 5% over the 0.5–7 keV range, most of the deviations are less than 3%. Residuals to simple fits to the other AGN (not shown) are also less than 3% over most of the 0.5–7 range and only as large as 5% near 0.7 keV. Thus, an approximate limit to relative systematic errors is about 3–5% over the HETGS range. While these residual errors will be examined further to see if they can be eliminated, another area of investigation will be the cross-dispersion selection efficiency, which is currently applied in the grating RMFs.

Recent HETGS Highlights

The High Energy Transmission Grating Spectrometer continues to provide excellent spectra for detailed examination of source properties. Over the past year, papers have appeared on warm ionized winds in AGN [2, 3, 8], the distance and dust to Cyg X-1[7], O star winds [5,6], and an accretion shock at the surface of V2129 Oph, a classical T Tauri star [4].

The T Tauri result is highlighted in Fig. 4, which shows the spatial distribution of the two X-ray emitting plasma components of V2129 Oph. Left and right cartoons correspond to the viewing angles of two *Chandra* observing segments, with observer in the rightward direction [4]. Red region marks the post-shock high density plasma at 3–4 MK, blue regions indicate low density coronal plasma with T ranging from 2 up to ~30 MK. The emission measure (EM) distributions derived from HETGS spectra corresponding to the two observing segments. Red EM bins symbolize observed EM values ascribed to post-shock plasma, while blue bins represent those accounting for coronal plasma. During segment 1, the pre-shock material does not block the view of both post-shock and coronal plasma: the EM distribution is therefore the sum of the EM distributions of the two components. During segment 2, the pre-shock material almost completely absorbs the X-rays of the post-shock plasma emitted toward the observer, while coronal emission is mostly unaffected: in this case, all the X-rays detected are those produced by coronal plasma; the reconstructed EMD, being only those of coronal plasma, hence misses the high EM values at 3–4 MK.

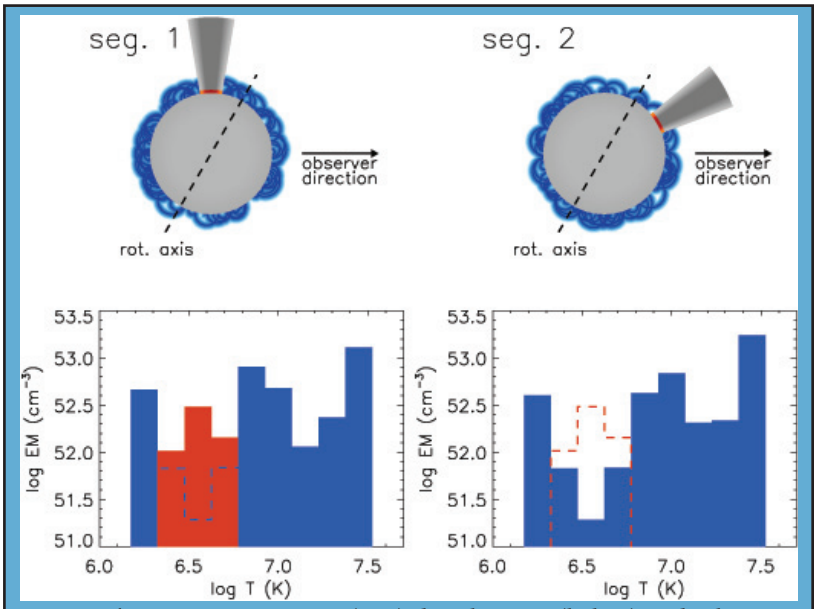

Fig. 4 - The emission measure (EM) distributions (below) and schematics of the physical model (above) are shown for two observations of the classical T Tauri star V2129 Oph. Most of the emission is from coronal gas (blue). EM with T of 3–4 MK is attributed to the base of the accretion stream (right panel, in red), observable in segment 1 but obscured by the upper part of the accretion stream during the 2nd observation (dashed red line in lower right panel). See Argiroffi et al. [4] for details.

References

[1] Perlman, E. S., et al. (2005). ApJ 625:727.
[2] Zhang, S. N., Ji, L., Marshall, H. L., et al. (2011). MNRAS 410:2274.
[3] Mocz, P., Lee, J. C., Iwasawa, K., & Canizares, C. R. (2011). ApJ 729:30.
[4] Argiroffi, C., Flaccomio, E., Bouvier, J., et al. (2011). A&A 530:A1.
[5] Mitschang, A. W., Schulz, N. S., Huenemoerder, D. P., Nichols, J. S., & Testa, P. (2011). ApJ 734:14.
[6] Cohen, D. H., Gagné, M., Leutenegger, M. A., et al. (2011). MNRAS 415:3354.
[7] Xiang, J., Lee, J. C., Nowak, M. A., & Wilms, J. (2011). ApJ 738:78.
[8] Zhang, S.-N., Gu, Q.-S., Ji, L., & Peng, Z.-X. (2011). Research in Astronomy and Astrophysics 11:1171.

LETG

Jeremy J. Drake, for the LETG Team

1. Ungainly Aging

Its not unusual for the aging process to cause things to sag and droop. We will not know how many *Chandra* years makes one human year until the mission ends, but hopefully its only about 3 or 4. There is no getting around it though: after 12 years in orbit *Chandra* is firmly in middle age.

The HRC-S was born a year or so before the *Chandra* launch, and its aging process began much earlier than

the rest of the spacecraft. On the ground it was subjected to subassembly calibration and "burn in" of the microchannel plates at count rates of thousands to tens of thousands of counts per second. Aging in orbit occurs when subjected to the 1700 V or so of tension between top and bottom microchannel plates during observations. This voltage serves to amplify the charge liberated by X-ray photon interactions with the top microchannel plate surface and its photoelectric effect-enhancing CsI coating. The resulting electron cascade within the pores of the plates is the signal that is detected and enhanced by amplifiers connected to a fine grid of wires situated beneath the plates. The magnitude of the signal for a given X-ray photon is referred to as the "pulse height" and is a measure of the gain of the instrument.

After years of use and bombardment by the ambient particle background, the plates "age", losing some of their photoelectic efficiency. This occurs primarily through chemical migration in the bottom plate where all the charge comes from. The net result is likely to be gain droop. Part of the routine monitoring of the HRC calls for regular observations of designated calibration sources whose behaviour is fairly constant and, if not, hopefully reasonable well-understood. For the HRC-S, the hot DA white dwarf HZ43 is the standard effective area monitoring source. It is thought constant and is the brightest source in the sky over much of the LETG+HRC-S wavelength range, providing useful signal from 50–170 Å in exposure times of 20 ks or so. We observe it every year and look at the count rates as a function of wavelength and detector position, and examine the pulse height distributions of the X-ray events.

Since launch we have observed a slow secular decline in the LETG+HRC-S count rates from HZ43. This meant either the discovery of exciting new white dwarf physics in which HZ43 is cooling at rates orders of magnitude faster than theory predicts, with startling implications for both astrophysics and physics in general. . . or a change in detector performance. We discovered the QE decline was accompanied by a slow decline in the event pulse height distributions—a sure sign of gain droop. The gain change itself did not matter too much, other than making the background filter Brad Wargelin had painstakingly developed based on X-ray pulse heights entertainingly more complex to implement. The QE decline was slow—just a bit more than 1% per year—and so practically inconsequential considering the absolute precision of the LETG+HRC-S effective area of about 15%. After accumulating a decade's worth of data we thought we had the QE decline well-characterized and included the effect in the *Chandra* calibration database by means of time-stamped detector quantum efficiency (QE) files: when generating effective areas for an observation in CIAO, the appropriate QE file for the time of the observation is incorporated automatically.

Perhaps unlike human aging, for detector aging grey is good. We want to see grey changes—changes that are essentially uniform with wavelength so that complex secular energy-dependent calibration models do not have to be constructed. The HRC-S QE decline looked grey, though at one time one of us who shall remain nameless (JJD) foolishly lost his house and all its contents on a bet that it was non-grey. It did in fact look grey until about two or so years ago, when we noticed that the longer wavelengths of the latest observed HZ43 spectra seemed slightly depressed compared with earlier trends. To define the trend, more data were needed (Fig. 1), and the non-grey QE drop is now quite obvious.

Why is the QE decline now non-grey? The bombardment by ambient particles produces photoelectrons and detectable signal, just as X-ray events do. The pulse height distribution for particles is quite different to that of X-ray photon events, and is essentially flat over the pulse height range of the former. However, most of the particle events have low pulse heights, and these events cause the full pulse height distribution to rise strongly at lower values. To avoid wasting valuable telemetry on these particle

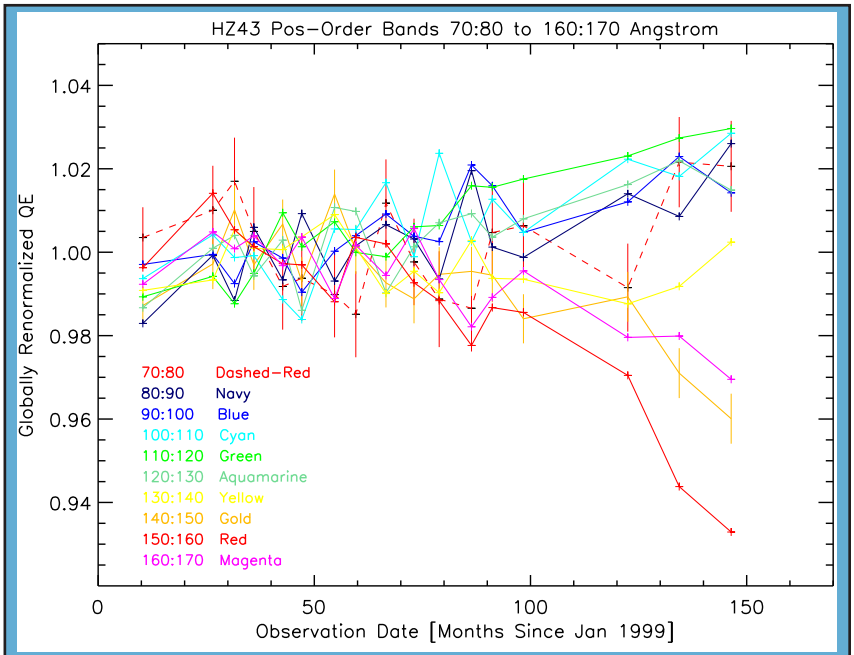

Fig. 1 - Gain droop on the HRC-S leads to loss of valid events in the longest wavelength channels. This mid-analysis figure made by "no gain without pain" expert Brad Wargelin shows trends in count rate for HZ43 in different wavelength regions. Note the relative decline at later times in the gold, red and magenta curves for $\lambda > 140$ Å.

events, they are filtered out onboard. Gain droop though has meant that the pulse heights of the lowest energy photon events are now beginning to merge with the background signal and some some are not being telemetered. In order to remedy this, we need to raise the detector gain—a face lift for the sagging. The gain can be increased by raising the high voltage between the front and rear plates, enhancing the electron cascade. It is not a trivial exercise however: taken too far, the high voltage could result in breakdown and arcing, potentially destroying the instrument. How did it turn out? See the HRC article on page 10 to find out.

2. Learning Curve

The LETG+HRC-S effective area curve relies, more than any of *Chandra*'s other instruments, on in-flight calibration using cosmic X-ray sources. *Chandra* was largely calibrated on the ground over many weeks through an extensive military-stye operation directed by Generals Weisskopf and Tananbaum at the MSFC X-ray Calibration Facility (XRCF). The best calibration data came from electron impact point sources (EIPS) in which an electron beam is accelerated onto an anode with sufficiently high voltage to excite "K-shell" transitions through removal of 1 s electrons. The X-ray spectrum of such a source usually has a nice bright K-line on top of a weaker continuum—a reasonable approximation to a monochromatic X-ray source (though the full X-ray spectral energy distribution generally had to be taken into account in analysis). The problem is that the energy spacing of K lines is rather sparse—C K at 0.28 keV, B at 0.18, Be at 0.11—and the HRC-S QE was not necessarily so slowly varying with energy that we could just join up the dots between the sparse measurements with straight lines.

XRCF was equipped with good monochromators that could be operated with continuum sources to select out nearly monochromatic X-rays of the desired energy. But the refections inside the monochromators tended to produce an X-ray beam that was not nearly as uniform as the beam from the EIPS alone. The calibration method, in essence, was to compare the detected signal in *Chandra*'s instruments with beam flux measured both at the telescope aperture and at some distance up-beam. The beam uniformity mattered because these beam measurements were spot measurements made by 4 flow proportional counters at the mirror entrance and one up-beam—again a problem of how to join the dots between the sparse measurements. In addition to these difficulties, the final in-flight high voltage settings of the HRC-S were optimized to slightly different values to those employed in ground calibration leading to expectations of different quantum efficiency between ground and flight conditions.

In Newsletter 13, I described some of the initial in-flight calibration of the LETGS based on hot white dwarf spectra (see Pease et al. (2000) for a more detailed description). *Chandra*'s low energy monitoring "standard candle" is the hot white dwarf HZ43. With a temperature of about 50,000 K, it is sufficiently hot to produce useful signal in the LETG+HRC-S down to about 50 Å or so. But as a single star, its surface gravity relied on spectral modelling in the UV-optical range. White dwarf X-ray fluxes are very sensitive to both the assumed effective temperature, and the surface gravity, and so a white dwarf with a better known mass was enlisted to help: Sirius B. The initial LETGS low energy in-flight calibration was, then, based on the spectra of HZ43 and Sirius B. Using the best models and stellar parameters of the day they did not quite agree where they overlapped though, and we had to do some guesswork to merge the two spectra and obtain what we thought was the best "average" effective area curve.

Subsequent years saw some improvements in the atmospheric models and in understanding the stellar fundamental parameters, and defects in the effective area model became apparent. The shorter wavelengths were re-calibrated using blazar spectra, taking advantage of overlap and cross-calibration with the HETG and ACIS-S detector—see Newsletters 16 and 17. Some foundations for a re-calibration at longer wavelengths using HZ43, Sirius B, and even assuming the spectrum of the isolated neutron star RXJ 1856 – 3754 might be a pure blackbody, were made by colleagues at LETG PI institutes MPE and SRON by Bauermann et al. (2006) and Kaastra et al. (2009). PhD student Benedikt Menz and long-time colleague Vadim Burwitz pioneered including another hot white dwarf, GD153, into the mix. With an effective temperature of 39000 K the latter bridges the effective temperature gap between HZ43 and Sirius B.

One result of all this work we took advantage of here was a growing confidence in parameters for HZ43 and that its spectrum was well-represented by pure hydrogen atmospheric models. We found that by co-adding 10 years' worth of HZ43 calibration data obtained since launch enabled us to obtain useful signal down to the C K edge, meeting up with our earlier blazar calibration. This offered a promising approach: the much cooler Sirius B X-ray model fluxes always seemed worryingly sensitive to fine details of the model atmosphere calculations and a calibration based on a single reference source—HZ43—held immense Occam's razor-like appeal. IT Specialist Nick Durham carefully accounted for the secular HRC-S QE decline, and reprocessed the data what must have seemed to him like several hundred times to account for small ~1% level tweaks and perfections in things like higher order contributions, extraction efficiencies and HRC deadtime

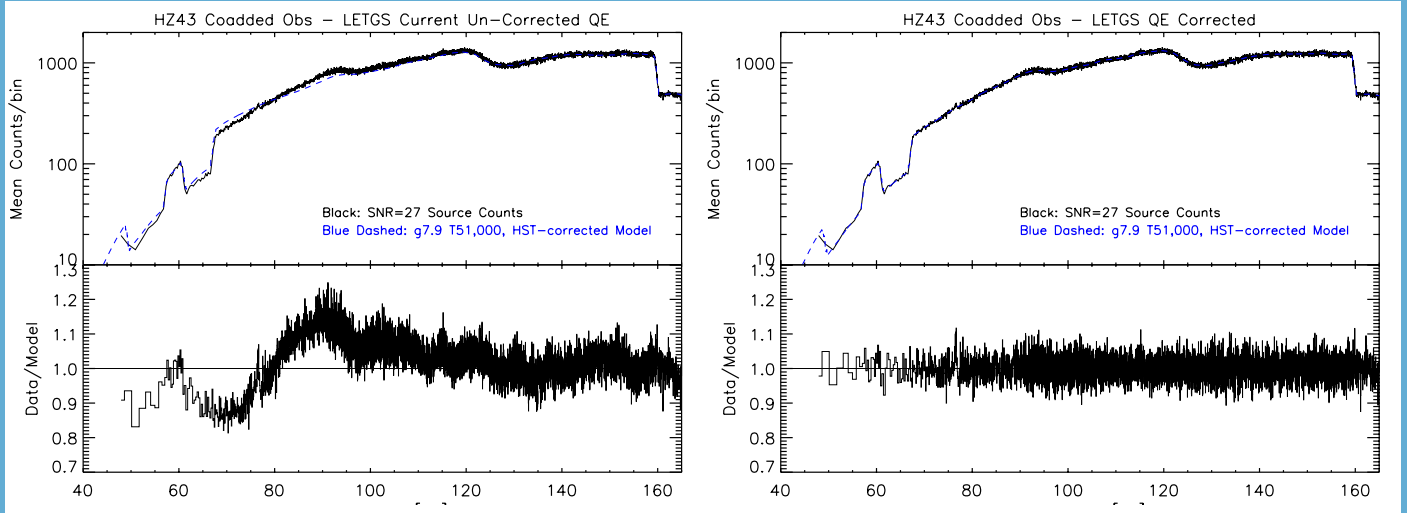

Fig. 2 - The before and after test of the new HRC-S QE model based on 10 years of accumulated HZ43 calibration data.

correction uncertainties. Data showing the non-grey gain sag were carefully excluded. The most up-to-date non-LTE pure hydrogen atmospheres available were computed by Thomas Rauch at the Eberhard Karls Universität Tübingen. Curves, bumps and wiggles in the data/model residuals were liposuctioned out and the QE smoothed out and stitched back together. The before and after comparison of residuals for HZ43 are illustrated in Fig. 2. The largest correction is the smoothing out of the S-shaped chicane in the residuals in the 60–90 Å region—a legacy from the earlier Sirius B-HZ43 compromise.

So, now that the HRC-S gain has been fixed, secular decline in QE is incorporated and it has been re-calibrated throughout its working range—covering a huge factor of 140 in energy—are we finished? Well, the problem is that the high voltage change to the detector will likely have an effect on the QE: once the optimum new settings have been established we will need to start over again. . .

JJD thanks Ralph Kraft and the LETG team for useful comments and discussion.

References

Beuermann, K., Burwitz, V., & Rauch, T. (2006). A&A 458: 541.
Kaastra, J. S., Lanz, T., Hubeny, I., & Paerels, F. B. S. (2009) A&A 497: 311
Pease, D. O., Drake, J. J., Johnson, C. O., et al. (2000). Proc. SPIE 4012:700.

Chandra Related Meetings

Check our website for details:
http://cxc.harvard.edu/

50 Years of X-ray Binaries
July 10–12, 2012
DoubleTree Guest Suites, Boston, MA
http://cxc.harvard.edu/cdo/xrb12/

Einstein Fellows Symposium
Fall 2012
http://cxc.harvard.edu/fellows/


X-ray Binaries
Celebrating 50 Years
Since the Discovery of Sco X-1
2012 Chandra Science Workshop
Hosted by the Chandra X-ray Center
July 10-12, 2012
at the DoubleTree Guest Suites Boston, MA
This meeting will celebrate the startling 1962 discovery of Scorpius X-1, the first X-ray source discovered outside the Solar System. The latest results in our understanding of X-ray binaries will then be explored probing mass accretion, jet formation, and other extreme physics in the environments close to black holes and neutron stars.
Deadline for Contributed Talk Abstracts
Wednesday, April 25, 2012
Deadline for Registration and Posters
Wednesday, May 23, 2012
Scientific Organizing Committee
Charles Bailyn Yale
Chris Done Durham
Andy Fabian IoA
Vicky Kalogera CIERA
Julia Lee Harvard
Tom Maccarone Southampton
Tod Strohmayer GSFC
Rashid Sunyaev MPA
Natalie Webb CESR
Andrea Prestwich* SAO
Peter Jonker* SRON
* SOC Chairs
Registration and Further Information
http://cxc.harvard.edu/cdo/xrb12/
xrb12@cfa.harvard.edu

Recent Updates to *Chandra* Calibration

Larry David

There were seven updates to the *Chandra* calibration database (CALDB) during 2011. These releases contained the standard quarterly calibration of the ACIS-S and ACIS-I gains and the yearly calibration of the HRC-I and HRC-S gains. While the QE of the HRC-I has been very steady, the QE of the HRC-S along the dispersion direction of LETG spectra has declined by about 5% during the *Chandra* mission. The QE at the location of the zeroth order in LETG spectra has declined by about 8%. The HRC-S QE decline has been accounted for by producing a separate QE map for each year since launch. The new HRC-S QE maps apply a grey correction, i.e., wavelength independent, to all HRC-S data. Yearly LETG/HRC-S observations of the white dwarf HZ43 show that the QE loss is essentially grey up to about 2009. More recent observations show that the HRC-S QE loss is more significant at longer wavelengths. This is discussed in more detail in the LETG artical on page 13.

During the past year, there were also updates to the HEG and MEG first order transmission efficiencies and the LEG higher order transmission efficiencies (m=2–10). The LEG updates were derived from a deep observation of the Crab nebula. With the latest LEG transmission efficiencies, the higher order fluxes are consistent with the first order flux to within 5–10%. By examining HETG/ACIS-S observations of a sample of about 30 AGN, we have derived corrections for the first order transmission efficiencies of both the HEG and MEG. Using those updated first order transmission efficiencies, the derived first order HEG and MEG fluxes are consistent to within about 5%.

The CXC calibration team has engaged in a number of internal cross-calibration studies over the past year. The supernova remnant G21.5-09 has been observed periodically by all four focal plane detectors over the course of the *Chandra* mission. Using the latest CALDB, the derived G21.5-09 fluxes for on-axis observations with the four focal plane detectors are consistent to within about 3%.

The *Chandra* calibration team continues to support the efforts of the International Astronomical Consortium for High Energy Calibration (IACHEC). Several CXC calibration scientists attended the 4th annual IACHEC meeing in Villa Grazioli, Italy between April 11–14, 2011. These meetings bring together calibration scientists from all present and most future X-ray and γ-ray missions. Collaborations among the calibration scientists have produced several papers that discuss the current cross-calibration status of the present fleet of X-ray telescopes. All of these papers have been published in Astronomy & Astrophysics and they contain a great deal of useful information for observers.

Useful *Chandra* Web Addresses

To Change Your Mailing Address:
http://cxc.harvard.edu/cdo/udb/userdat.html

CXC:
http://chandra.harvard.edu/

CXC Science Support:
http://cxc.harvard.edu/

CXC Education and Outreach:
http://chandra.si.edu/

ACIS: Penn State
http://www.astro.psu.edu/xray/axaf/

High Resolution Camera:
http://hea-www.harvard.edu/HRC/HomePage.html

HETG: MIT
http://space.mit.edu/HETG/

LETG: MPE
http://www.mpe.mpg.de/xray/wave/axaf/index.php

LETG: SRON
http://www.sron.nl/divisions/hea/chandra/

CIAO:
http://cxc.harvard.edu/ciao/

Chandra Calibration:
http://cxc.harvard.edu/cal/

MARX simulator
http://space.mit.edu/ASC/MARX/

MSFC: Project Science:
http://wwwastro.msfc.nasa.gov/xray/axafps.html

CIAO 4.4

Improved tools, a new graphical user interface for plotting and advanced Sherpa functionality

Antonella Fruscione, for the CIAO Team

The newest versions of the *Chandra* Interactive Analysis of Observations software and the *Chandra* Calibration Database (Version 4.4 of CIAO and CALDB 4.4.7), were released in December 2011 (*http://cxc.harvard.edu/ciao*). These include numerous enhancements and bug fixes with respect to previous CIAO versions, all listed in detail in the software release notes. We will describe here some of the most notable changes and improvements.

CIAO Tools

• `acis_find_afterglow` is a new tool which improves over previous algorithms by identifying shorter afterglows as well as ones with larger gaps between the events comprising them.

A cosmic-ray "afterglow" is produced when a large amount of charge is produced by interaction with a charged particle. Most of the charge is clocked off of the CCD in a single frame. However, a small amount can be captured in charge traps, which release the charge relatively slowly. As a result, a sequence of events can appear in a single pixel over a few to even a few dozen frames, and the events do not necessarily occur in consecutive frames; there can be gaps of several frames with no events for the pixel. In general, the amount of charge released per frame declines with time. However, the trend is not monotonic, especially near the end of an afterglow. More details on afterglows, afterglow-identification algorithms and how to display the afterglow events can be found in the "Why Topic" "Cosmic-Ray Afterglows" at *http://cxc.harvard.edu/ciao/why/afterglow.html*

The tool `acis_find_afterglow` searches for afterglows using a short, sliding time window. If there is a statistically significant excess of events compared to the expected number of background events, then the excess is identified as an afterglow unless the excess seems to be associated with a source that is periodically dithered across the pixel. The algorithm used to estimate the nominal number of background events is designed to avoid contamination by bright sources. Essentially all of the afterglows that have four or more events are identified by `acis_find_afterglow`. The tool `acis_find_afterglow` also searches for hot pixels, using an algorithm that is similar to the afterglow-identification algorithm except that the time window used is the entire duration of an observation. Events associated with afterglows are ignored during the search for hot pixels. The tool `acis_find_afterglow` supersedes the tools `acis_classify_hotpix`, `acis_detect_afterglow`, `acis_find_hotpix`, and `acis_run_hotpix` for all analyses.

• The Mexican-Hat Wavelet source detection tool `wavdetect` now takes an observation-specific PSF map file (created for example with `mkpsfmap`) instead of using *Chandra* PSF table data from the CALDB. Data from other missions (e.g. ROSAT, *XMM-Newton*) can also be supported by providing a psfmap (see "ahelp `wavdetect`" for more details).

• The `addrsp` tool adds together multiple imaging ARFs (auxiliary response files) and RMFs (response matrix files) to create a pair of merged ARF and RMF files weighted by ARFs and exposure. The tool may be run with just ARF files as input to create a merged ARF weighted by exposures. The `addresp` tool may now be used to combine grating ARFs, creating the same output as the `dmarfadd` tool. We have also added support for combining the ARF and RMF into an RSP file instead of making two separate files.

• The `asphist` tool bins the aspect solution of an observation into a 3D histogram of duration vs x and y pointing offset and roll offset. The value in each bin is the time the pointing was within that offset bin during the observation, as modified by the good-time interval (GTI) and dead-time-correction factor (DTF). The updated algorithm uses the full tangent plane offset computations and the correct angle between pointing and North. Both of these changes improve the accuracy of data reprojected to different tangent points and/or combined from multi-obi observations with significantly different pointings.

CIAO Scripts

The CIAO contributed scripts package (*http://cxc.harvard.edu/ciao/download/scripts/*) is considered a required part of the software installation and contains analysis scripts and modules written by scientists at the CXC. The contributed scripts and modules automate repetitive tasks and extend the functionality of the CIAO software package by filling specific analysis needs. The package is updated about once a month and concurrently with major CIAO releases. For CIAO 4.4. all scripts were retested to ensure a smooth running within the new system. Some scripts, including specifically `Chandra_repro`, `combine_spectra` and `specextract`, were upgraded to use the new tools and features of CIAO 4.4. For example, `Chandra_repro` is using the new tool `acis_find_afterglow` in place of `acis_run_hotpix` to identify

cosmic ray afterglows and bad pixels in ACIS observations. In `combine_spectra`, users can now specify whether the script should sum or average the PHA exposure times for the header of the combined spectrum and ARF files. In `specextract`, a binning of the sky2tdet WMAP (used as input to the tool `mkwarf`) can now be specified: this is useful for example when making a weighted ARF for a large region.

The script package has been updated after CIAO 4.4 with a new script `splitroi`, for splitting the source and background regions created by the roi ("region of interest") tool, and a new module, `crates_contrib.utils`, with new routines helpful within CRATES (the software package developed by the CXC to provide a high level I/O interface for use by Python). Most likely by the time of printing, further updates to the script package will be available.

CHIPS

ChIPS (*http://cxc.harvard.edu/chips/*) is the imaging and plotting platform for CIAO which can be used during data analysis—e.g. to plot a lightcurve or a spectrum—and to create publication-quality figures. ChIPS is designed for use in a variety of modes: as a user-interactive application and in batch mode. ChIPS is an importable module for the Python scripting language and is available as a C/C++ library for software developers. The major updates in the CIAO 4.4 release are the inclusion of a new ChIPS graphical user interface (the ChIPS GUI) and improvements to the PDF support (e.g. to support the alpha and opacity settings of images, regions, and histograms). The ChIPS GUI

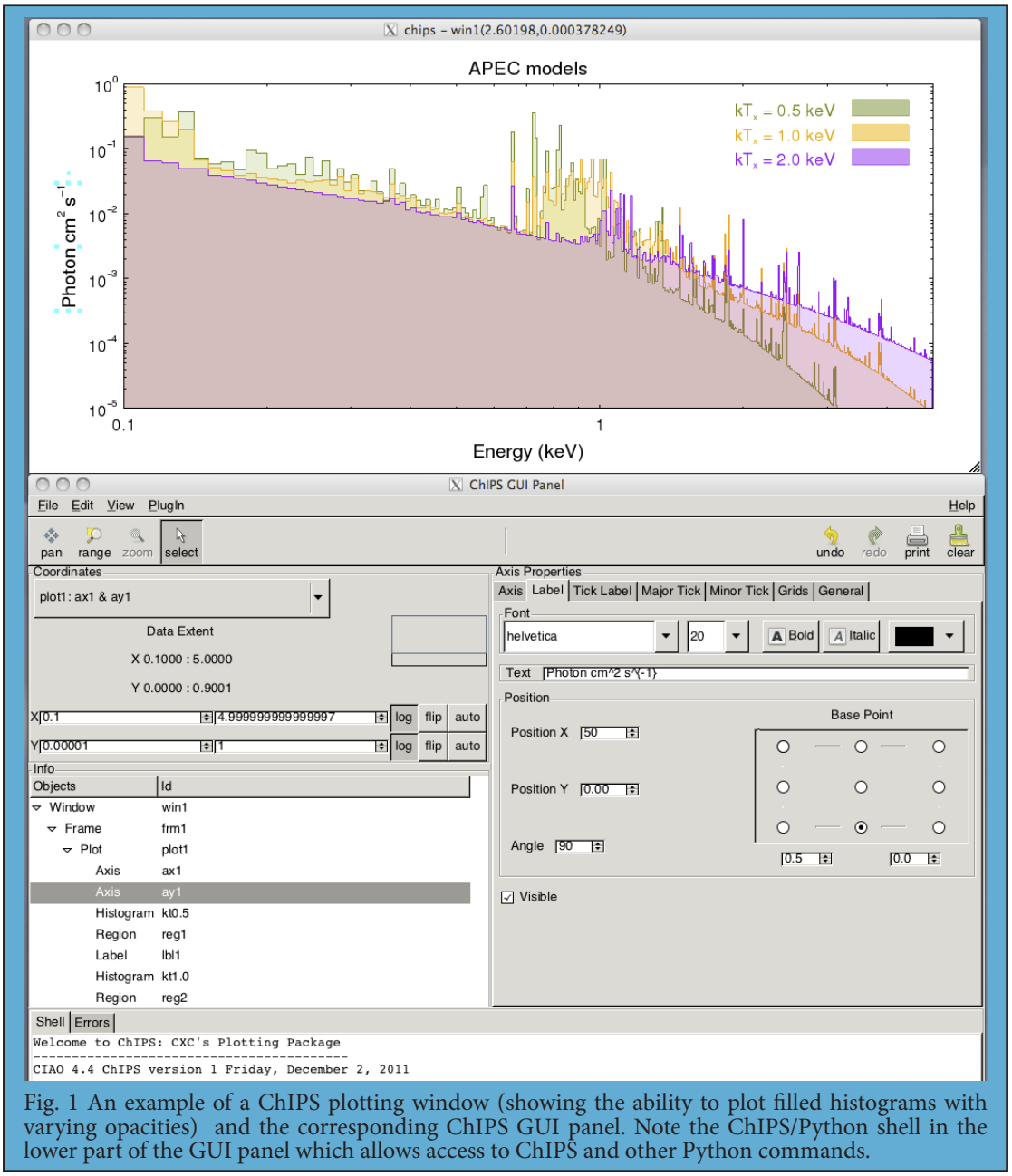

Fig. 1 An example of a ChIPS plotting window (showing the ability to plot filled histograms with varying opacities) and the corresponding ChIPS GUI panel. Note the ChIPS/Python shell in the lower part of the GUI panel which allows access to ChIPS and other Python commands.

(Fig.1) allow users to adjust the layout of their plots and make edits to many of the plot properties. A Python terminal is built into the GUI, allowing access to ChIPS and other Python commands. The GUI is available to any process that creates a ChIPS plot, such as Sherpa and Prism. It can be launched by right-clicking on on an existing ChIPS window and selecting "Show GUI", or by running the `show_gui` command from the ChIPS command line. Currently the GUI allows users to edit the properties of existing visualizations but does not provide the ability to add or create new objects.

A large gallery of ChIPS examples is included in the ChIPS website at *http://cxc.harvard.edu/chips/gallery/* and there are a number of introductory threads to guide beginners.

SHERPA

Sherpa (*http://cxc.harvard.edu/sherpa/*) is the modeling and fitting application within CIAO that can be used for analysis of images, spectra and time series from many telescopes, including optical telescopes such as *Hubble*. Sherpa is flexible, modular and extensible. It has an IPython user interface and is also an importable Python module. Sherpa models, optimization and statistical functions are available via both C++ and Python for software developers wishing to link such functions directly to their own compiled code. Important changes and additions to the Sherpa functionality in the CIAO 4.4 release are described in a dedicated webpage at *http://cxc.harvard.edu/sherpa/updates.html* Among the several improvements to the software, we highlight two advanced features below.

Bayesian Analysis with pyBLoCXS

pyBLoCXS, a sophisticated Markov chain Monte Carlo based algorithm designed to carry out Bayesian Low-Count X-ray Spectral (BLoCXS, van Dyk, et al. 2001) analysis in the Sherpa environment, is available via several new Sherpa functions. The algorithm explores parameter space at a suspected minimum, using a predefined Sherpa model applied to high-energy X-ray spectral data. pyBLoCXS supports the ability to flexibly define priors and allows for variations in the calibration information. It can be used to compute posterior predictive p-values for the likelihood ratio test (Protassov et al. 2002) .

Template Models

Sherpa supports a new template model (an extension of the table model). Sherpa can now read in a collection of templates from a directory full of template files, and can compare a data set to all the templates in that collection. Sherpa finds the template that best matches the data, and reports back the parameter values associated with that template. The gridsearch optimization method will select the best template model by trying all of the templates. This method evaluates the fit statistic for each point in the parameter space grid; the best match is the grid point with the lowest value of the fit statistic. Gridsearch reports back the parameter values associated with this point. The Sherpa template model supports nearest-neighbor and polynomial interpolation.

Users interested in hands-on CIAO training should plan to attend a future CIAO workshop at the *Chandra* X-Ray Center. More information will be posted at *http://cxc.harvard.edu/ciao/workshop/* when available.

More information and updates on CIAO can always be found at *http://cxc.harvard.edu/ciao/* or subscribe to the CIAO News RSS feed at *http://cxc.harvard.edu/ciao/feed.xml*

To keep up-to-date with CIAO news and developments subscribe to chandra-users@head.cfa.harvard.edu (send e-mail to 'majordomo@head.cfa.harvard.edu', and put 'subscribe chandra-users' (without quotation marks) in the body of the message).

References

Protassov, R., van Dyk, D.A., Connors, A., Kashyap, V.L., Siemiginowska, A. (2002). ApJ 571:545.
van Dyk, D.A., Connors, A., Kashyap, V.L., & Siemiginowska, A. (2001). ApJ 548:224.

The Results of the Cycle 13 Peer Review

Belinda Wilkes

The observations approved for *Chandra*'s 13th observing cycle are now in full swing and the Cycle 14 Call for Proposals (CfP) was released on 15 December 2011. Cycle 12 observations are close to completion.

The Cycle 13 observing and research program was selected as usual, following the recommendations of the peer review panels. The peer review was held 21–24 June 2011 at the Hilton Boston Logan Airport. More than 100 reviewers from all over the world attended the review, sitting on 15 panels to discuss 664 submitted proposals (Fig. 1). The Target Lists and Schedules area of our website provides lists of the various types of approved programs, including abstracts. The peer review panel organization is shown in Table 1.

The Cycle 13 CfP included a call for X-ray Visionary Projects (XVPs) for the first time. XVPs are major, coherent science programs to address key, high-impact scientific questions in current astrophysics and requiring 1–6 Ms of observing time. A larger amount of observing time available due to the lower fraction of an orbit spent within the radiation belts over the next 2–3 years as *Chandra*'s orbit evolves. As a result, the observing time available for GO proposals and Large Projects (LPs) was not impacted by the XVP allocation. The total amount of time allocated in Cycle 13 was close to 27 Ms, including 8 Ms awarded to 4 XVPs and 4.7 Ms to 11 LPs. The response to the new XVP opportunity was very positive. The over-subscription for LPs and XVPs was 7.4 and 7.1 respectively. The overall over-subscription in observing time was 5.4 (Fig. 2), typical of the past few cycles despite the much larger amount of time being allocated (Fig. 3). The continued evolution of the *Chandra* orbit has allowed us to again include XVPs in the Cycle 14 CfP.

As is our standard procedure, all proposals were reviewed and graded by the topical panels, based primarily upon their scientific merit, across all proposal types. The topical panels produced a rank-ordered list along with detailed recommendations for individual proposals where relevant. A peer review report was drafted for each proposal by one/two members of a panel and edited by the Deputy panel chair before being delivered to the CXC. The topical panels were allotted *Chandra* time to cover the allocation of time for GO observing proposals based upon the demand for time in that panel. Other allocation limits for each panel were: joint time, TOOs with a < 30 day response, time constrained observations in each of 3 classes and money to fund archive and theory proposals. Many of these allocations are affected by small number statistics in individual panels so allocations were based on the full peer review over-subscription ratio. Panel allocations were modified, either in realtime during the review or after its completion, to transfer unused allocations between panels as needed.

Table 1: Panel Organization

Topical Panels:	
<u>Galactic</u>	
Panels 1,2	Normal Stars, WD, Planetary Systems and Misc
Panels 3,4	SN, SNR + Isolated NS
Panels 5,6,7	WD Binaries + CVs, BH and NS Binaries, Galaxies: Populations
<u>Extragalactic</u>	
Panels 8,9,10	Galaxies: Diffuse Emission, Clusters of Galaxies
Panels 11,12,13	AGN, Extragalactic Surveys
XVP Panel	XVP Panel X-ray Visionary Proposals
Big Project Panel	LP and XVP Proposals

LPs and XVPs were discussed by the topical panels and ranked along with the GO, archive and theory proposals. In addition, the XVPs were also discussed and ranked by a separate XVP/pundit panel. The topical and XVP panels' recommendations were recorded and passed to the Big Project Panel (BPP), which includes all topical panel chairs and members of the XVP panel. The BPP discussed the LPs and XVPs separately and generated two rank-ordered lists.

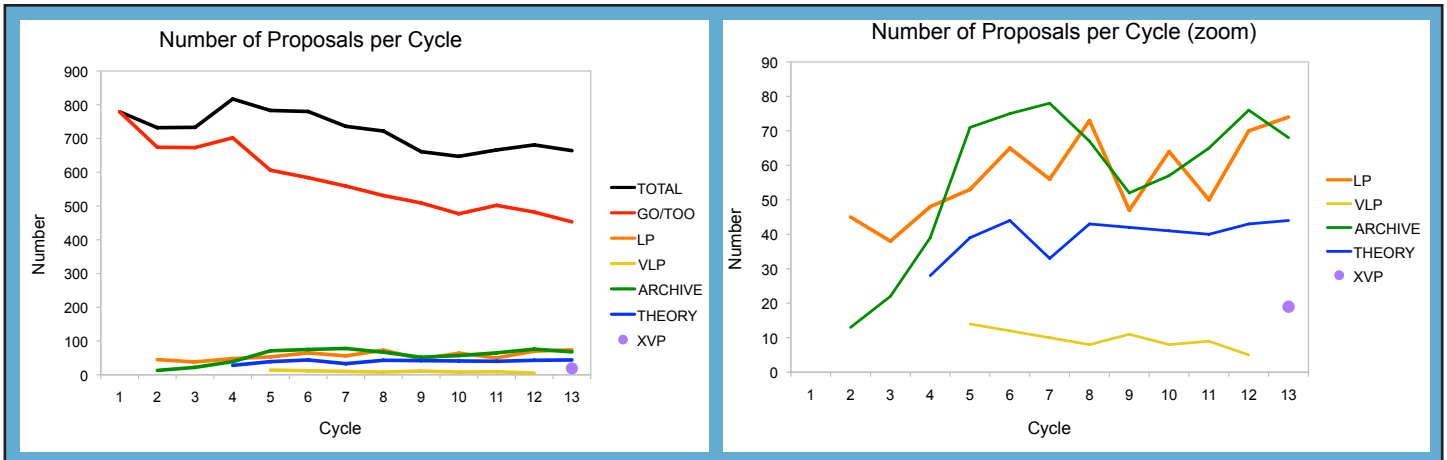

Fig. 1: (Left) The number of proposals submitted by proposal type (e.g. GO, LP, Archive etc.) as a function of cycle. (Right): zoom on lower curves. Since more proposal types have become available in each cycle, the number classified as GO has decreased as other types increase. The total number of submitted proposals is remarkably constant.

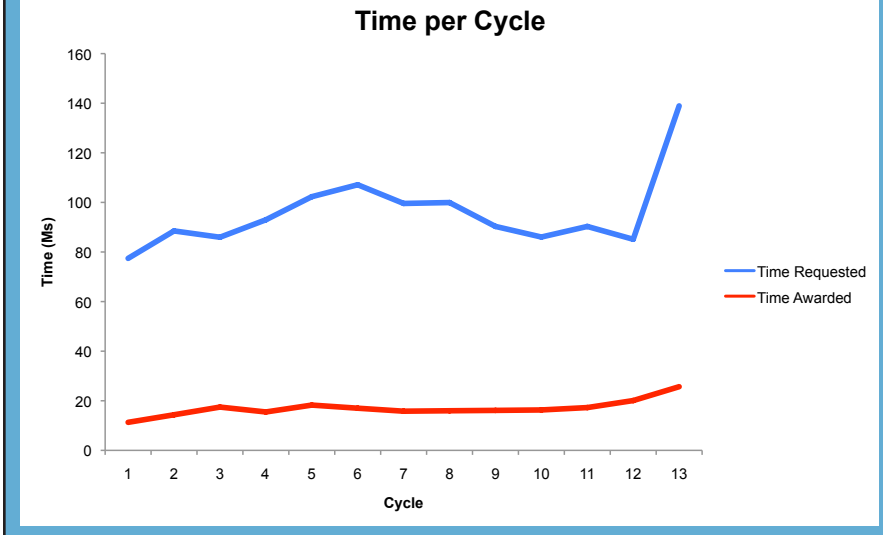

Fig. 2: The requested and approved time as a function of cycle in Msecs. This increased in the first few cycles, the largest effect being due to the introduction of Very Large Projects (VLPs) in Cycle 5. The increase in requested and awarded time in Cycle 13 is clear.

BPP panelists updated review reports, as needed, at the review and remotely over the following 2 weeks. The schedule for the BPP at the review included time for reading and for meeting with appropriate panel members to allow coordination for each subject area. The BPP meeting extended into Friday afternoon to allow for additional discussion and a consensus on the final rank-ordered lists to be reached.

The resulting observing and research program for Cycle 13 was posted on the CXC website on 15 July 2011, following detailed checks by CXC staff and approval by the Selection Official (CXC Director). All peer review reports were reviewed by CXC staff for clarity and consistency with the recommended target list. Formal e-letters informing the PIs of the results, budget information (when appropriate) and providing a report from the peer review, were e-mailed to each PI in early August.

Joint Time Allocation

Chandra time was also allocated to several joint programs by the proposal review processes of *XMM-Newton* (4 proposals) and *Spitzer* (2 proposals).

The *Chandra* review accepted joint proposals with time allocated on: *Hubble* (20), *XMM-Newton* (4), NRAO (12), and NOAO (2).

Constrained Observations

As observers are aware, the biggest challenge to efficient scheduling of *Chandra* observations is in regulating the temperature of the various satellite components (see POG Section 3.3.3). In Cycle 9 we instituted a classification scheme for constrained observations which accounts for the difficulty of scheduling a given observation (CfP Section 5.2.8). Each constraint class was allocated an annual quota based on our experience in previous cycles. The same classification scheme was used in Cycles 10–13. In Cycle 13, the quotas were increased commensurate with the larger amount of observing time to be awarded. There was a large demand for constrained time so that not all proposals which requested time-constrained observations and had a passing rank (>3.5) could be approved. Effort was made to ensure that the limited number of constrained observations were allocated to the highest-ranked proposals review-wide. Detailed discussions with panel chairs enabled us to record the priorities of their panels in the event that more constrained observations could be allocated. Any remaining uncertainty concerning priorities during the final decision process

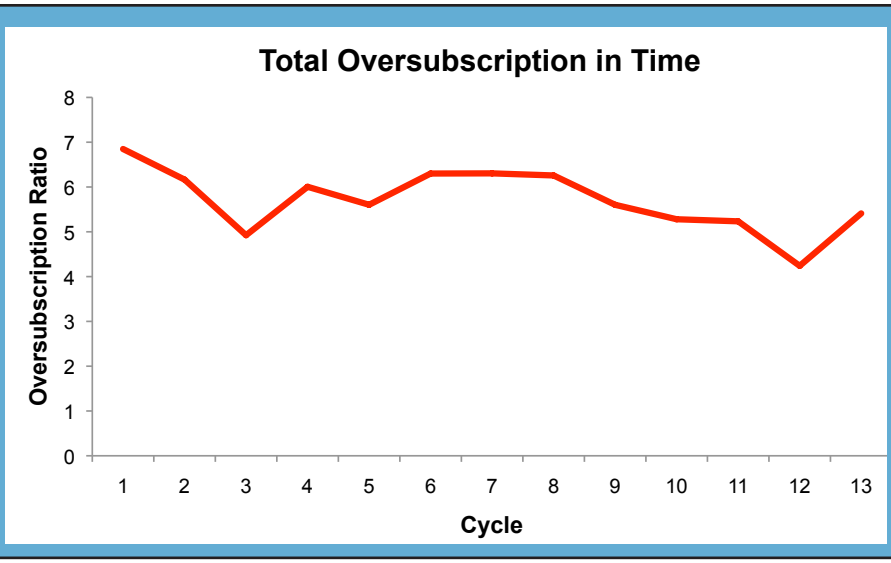

Fig. 3: The final oversubscription in observing time based on requested and allocated time in each cycle. Again the numbers are remarkably constant. The decrease in Cycle 12 reflects the 16% larger amount of time awarded by the peer review in that cycle to offset the significantly increasing observing efficiency as the orbit evolved (see article in 2011 Newsletter).

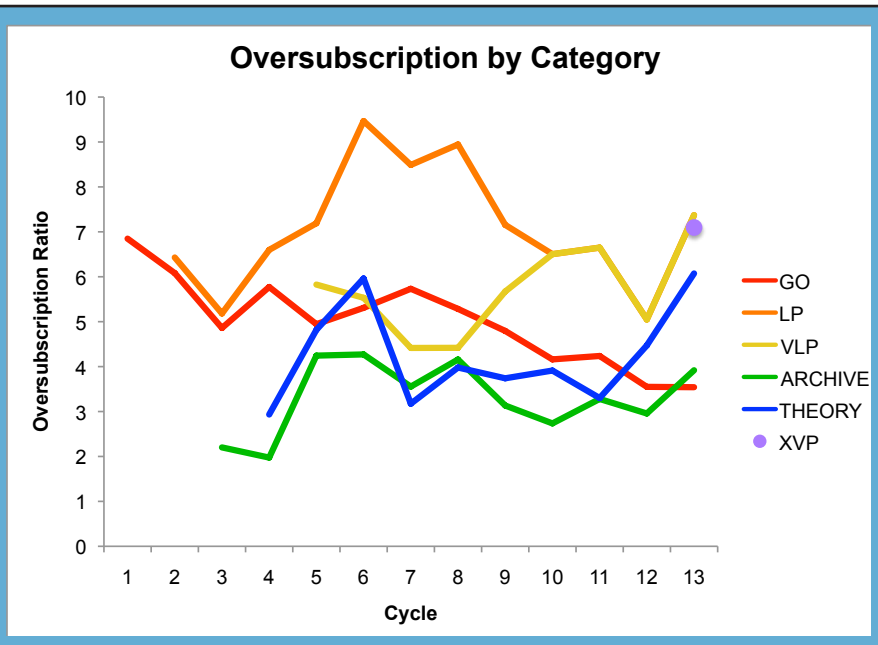

Fig. 4: The effective over-subscription ratio in terms of observing time for each proposal type as a function of cycle. Archive and Theory proposal over-subscription is against available funding. Please note that some of the fluctuations are due to small number statistics (e.g. Theory proposals).

was discussed with the relevant panel chairs before the recommended target list was finalized.

The same 3 constraint classes will be retained in Cycle 14 so as to ensure a broad distribution in the requested contraints. We urge proposers to specify their constraints as needed by the science.

Early Start for Cycle 13 Observations

Cycle 13 observations began early this year, in July/August, due to the continuing fall-out from the spacecraft "MUPS anomaly," during the summer of 2009 (described in the 2010 Newsletter) which resulted in many of the summer Cycle 11 targets being observed during the summer of 2009. The resulting lack of Cycle 12 summer targets in 2011 meant that Cycle 13 summer targets were needed to maintain an efficient schedule. An announcement was distributed in May 2011 informing Cycle 13 proposers that they may be called upon for fast turnaround in checking and confirming their observation parameters to allow observation in the summer. Due to the excellent response of observers and the diligence of the User Interface and Mission Planning teams, the updated procedures ran smoothly and an efficient schedule was maintained throughout the summer and beyond.

Cost Proposals

PIs of proposals with US collaborators were invited to submit a Cost Pro- posal, due in Sept 2011 at SAO. In Cycle 13 each project was allocated a budget based on the details of the observing program (see CfP Section 8.4). Awards were made at the allocated or requested budget levels, whichever was lower.

Given the early start of observations, we modified our procedures to facilitate early award of cost proposals with observations made in July and August. Complete proposals submitted before the 7th September deadline and for which observations had already been made were treated as high priority, processed and awarded in mid-October.

The remainder of the award letters were emailed in late October and November, in good time for the official start of Cycle 13 on 1 Jan 2012.

Proposal Statistics

Statistics on the results of the peer review can be found on our website: under "Target Lists and Schedules:"

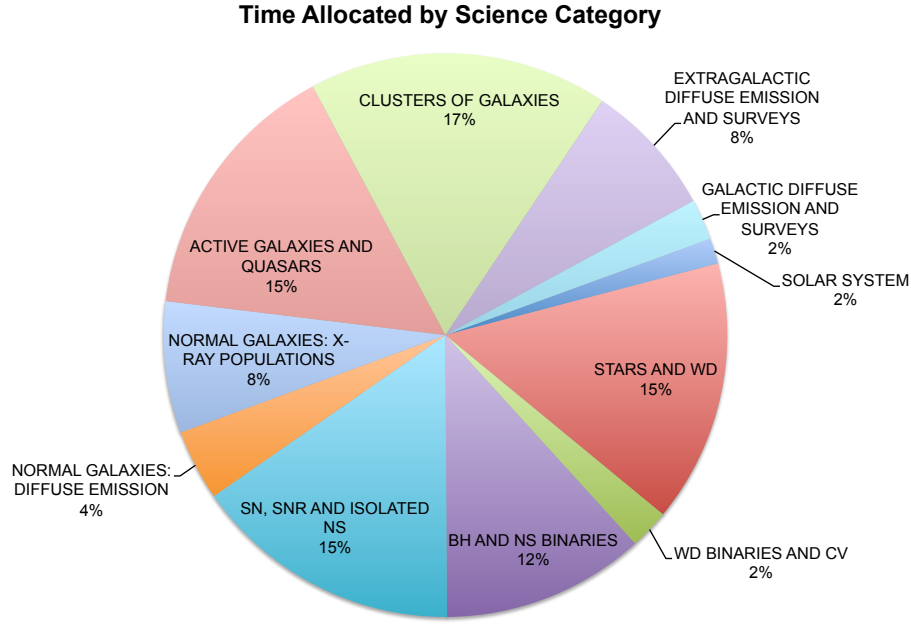

Fig. 5: A pie chart indicating the percentage of *Chandra* time allocated in each science category. Note that the time available for each category is determined by the demand.

select the "Statistics" link for a given cycle. We present a subset of those statistics here. Fig. 4 displays the effective over-subscription rate for each proposal type as a function of cycle. Figs. 5, 6 show the percentage of time allocated to each science category and to each instrument combination. Table 2 lists the numbers of proposals submitted and approved by country of origin.

Table 2: Number of Requested and Approved Proposals by Country

Country	Requested		Approved	
	# Proposals	Time (ksec)	# Proposals	Time (ksec)
USA	493	112744.5	149	21591.0
Foreign	171	29150.5	50	5178.0

Country	Requested		Approved	
	# Proposals	Time (ksec)	# Proposals	Time (ksec)
Argentina	2	200.0		
Australia	5	860.0	1	150.0
Belgium	1	250.0		
Canada	10	887.0	3	111.0
Chile	1	278.0		
China	2	464.0		
Denmark	1	160.0		
France	10	1085.0	5	345.0
Germany	19	7343.0	5	405.0
Hong Kong	1	10.0		
India	6	640.0	1	40.0
Israel	1	180.0		
Italy	36	6144.0	9	849.0
Japan	9	917.0	2	200.0
Korea	1	262.0		
Netherlands	15	1470.0	4	630.0
Russia	2	94.0		
S. Africa	2	1044.0		
Spain	9	1140.0	5	480.0
Switzerland	1	50.0	1	50.0
Taiwan	3	281.0	3	281.0
Turkey	1	75.0		
U.K.	33	5316.5	11	1687.0

* Note: Numbers quoted here do not allow for the probability of triggering TOOs

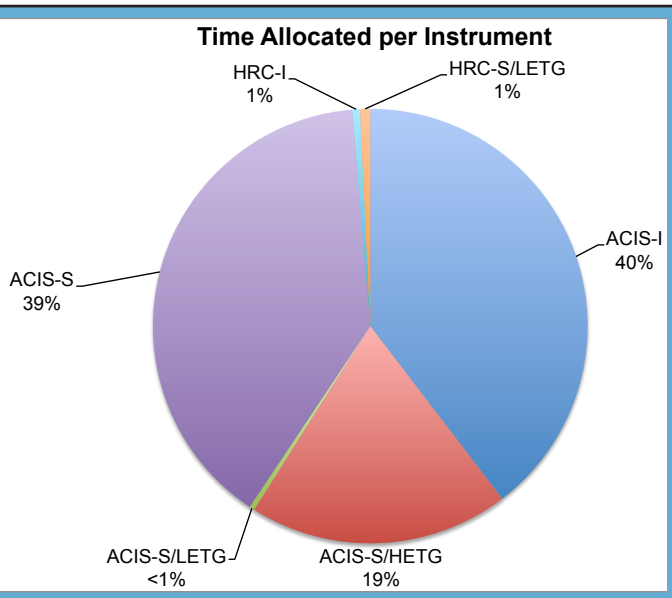

Fig. 6 : A pie chart showing the percentage of *Chandra* time allocated to observations for each instrument configuration.

The Einstein Fellowship Program

Andrea Prestwich

The past year has been busy for the Einstein Fellowship Program Office. In July 2011 we released the Call for Proposals for the 2012 class of Einstein Fellows—the third year of the Einstein program. We had a bumper crop of 189 applicants for 12 Fellowships. The selection panel met in January 2012 and had an extremely tough job selecting the winners! At the time of writing (February 2012) offers have gone out and are eagerly awaiting responses! The annual Einstein Fellows Symposium was held at NASA-GSFC in October 2011 hosted by *Fermi* Project Scientist Julie McEnery. As always, the talks were terrific and the Symposium was well attended by scientists from Goddard and others in the DC area.

The Einstein Fellows web pages, at *http://cxc.havard.edu/fellows/*, have been re-designed over the past year. The two main changes are new biographies for current Fellows and a News section. The intention of the news section is to showcase the wonderful accomplishments of the Fellows and to keep applicants informed as to the status of the selection process. To that end we posted the dates of the selection panel meeting and updated the site as soon as offers were made and those on the wait-list notified.

Job-hunting can be extremely stressful, and we hope that

these updates will alleviate some of the uncertainty. We took a hard look at the Fellowship Terms and Conditions and decided that we could add wording allowing for up to 12 weeks of unpaid leave for family or medical reasons. This brings us in-line with the Family and Medical Leave Act. Since Fellows are not employees but receive a stipend, in practice this means that we "stop the clock" for up to 12 weeks and extend the Fellowship beyond the nominal stop date. We hope this will give some flexibility to deal with family issues.

Einstein Fellows have had some notable successes over the past year. Eran Ofek (2009) has moved back to Israel to take up a faculty position at the Weizmann Institute of Science. Nico Yunes (2010) and Dovi Poznanski (2010) have accepted faculty positions at Montana State University and Tel Aviv University in Israel respectively. Tamara Bogdanovic (2010) has been offered a faculty position at Georgia Tech School of Physics upon completion of her fellowship. When I read the end of year reports I'm always astonished by the productivity of our Fellows, but two recent papers merit special mention. Matthew Kerr (2011), Robin Corbet, Teddy Cheung, and the *Fermi* LAT collaboration have a recent (January 2012) paper in Science reporting on the discovery of periodic emission from the gamma-ray binary 1FGL J1018.6-5856. This object is one of only three gamma binaries known and the first to be discovered by the LAT by searching for a period. The work of Kevin Schawinski (2009) describing a "young" supermassive black hole was showcased in a recent press release from Yale University (*http://news.yale.edu/2011/12/01/yale-discovery-young-supermassive-black-holes-challenges-current-theory*). Congratulations to all the Fellows on a great year, and we're looking forward to 2012!

Got Data—Will Publish!

Arnold Rots, Sherry Winkelman, Glenn Becker

The *Chandra* Data Archive's bibliography database (*http://cxc.harvard.edu/cgi-gen/cda/bibliography*) provides its users not only with a powerful research tool, it also allows us to track what happens to all the valuable *Chandra* observations.

Rather than asking how many papers were published on *Chandra* observations or how many citations they received, we started wondering how much of the *Chandra* data actually result in refereed journal articles and how often. After a fair bit of experimentation we constructed the graph in Fig. 1. It shows what fraction of the available *Chandra* exposure time was published—once, twice, thrice, or more often—as a function of the data's age, in steps of one year.

The figure represents the status on 1 August 2011 and includes all non-calibration and non-engineering observations that were made prior to 1 August 2010. More precisely, it shows what percentage of exposure time that has been available for *N* years or more, was presented in a paper in a refereed journal, *N* years after the observation was first released to the PI.

It turns out that this figure, notwithstanding its simplicity, yields a lot of information:

- Second publications start about a year after the first, indicative of the common one-year proprietary period.
- It takes about two and a half years for half the data to be published.
- After four years the curve starts to flatten.
- At seven years about 85% of the data have been published and we have nearly reached an equilibrium. This is a very high percentage.
- Also at seven years, 50% of the data have been published more than twice, indicative both of the popularity of the archive, and the utility of the data.
- Beyond ten years the percentage of data published exceeds 90%. However, since that range pertains pretty much to the data from the early days of the mission, we are curious to see whether such a percentage will be sustained for the later years, too.

Similar statistics are not available for other missions or observatories, but we are confident that the high percentage of data that gets published represents a high score, confirming that *Chandra* data are judged extremely valuable by its user community. Similarly, the statistics on multiple publications is indicative of the intensive use that the community makes of the *Chandra* Data Archive.

A more extensive paper on the Chandra publication statistics will appear in the April 2012 issue of PASP (Volume 124, No. 914).

This kind of information is available thanks to the extensive bibliographic database that the Archive Operations Team maintains. We are grateful for the help we receive from users who provide in their papers explicit information on which observations they use. We would like to encourage all *Chandra* Guest Observers and users of the *Chandra* Data Archive to follow their example or, even better, to embed Dataset Identifiers in their manuscripts (see *http://cxc.cfa.harvard.edu/cda/datasetid.html)*.

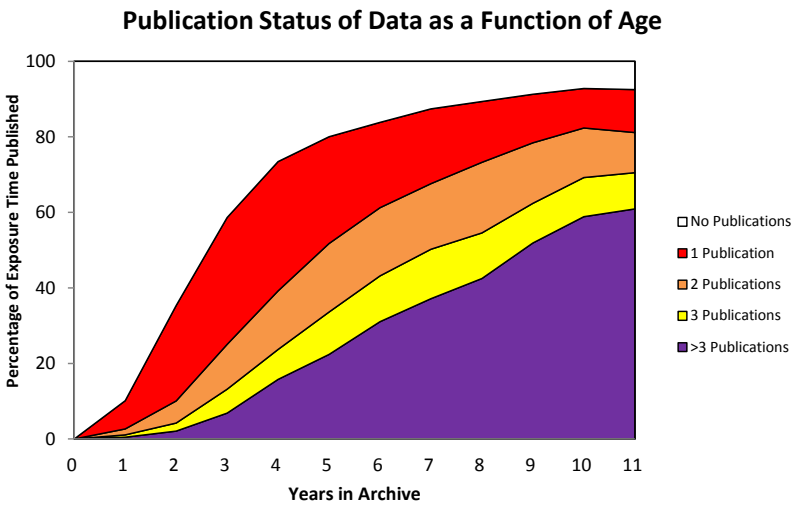

Fig. 1 - Percentage of the available *Chandra* time published as a function of the data's age.

Chandra Users' Committee Membership List

The Users' Committee represents the larger astronomical community for the *Chandra* X-ray Center. If you have concerns about *Chandra*, contact one of the members listed below.

Name	Organization	Email
Lee Armus	SSC	lee@ipac.caltech.edu
Franz Bauer	SSI	fbauer@spacescience.org
Tiziana DiMatteo	CMU	tiziana@lemo.phys.cmu.edu
Erica Ellingson	CASA-Colorado	erica.ellingson@colorado.edu
Jimmy A. Irwin	University of Alabama	jairwin@ua.edu
Tim Kallman	GSFC	Timothy.R.Kallman@nasa.gov
Hironori Matsumoto	Nagoya University	matumoto@u.phys.nagoya-u.ac.jp
Jon Miller (Chair)	University of Michigan	jonmm@umich.edu
Pedro Rodriguez	ESA	prodrigu@sciops.esa.int
Massimo Stiavelli	STScI	mstiavel@stsci.edu
John Tomsick	UC Berkeley	jtomsick@ssl.berkeley.edu
Joan Wrobel	NRAO	jwrobel@nrao.edu
Ex Officio, Non-Voting		
Jaya Bajpayee	NASA HQ	jaya.bajpayee-1@nasa.gov
Wilt Sanders	NASA HQ	wsanders@hq.nasa.gov
Allyn Tennant	NASA/MSFC, Project Science	allyn.tennant@msfc.nasa.gov
Martin Weisskopf	NASA/MSFC	martin@smoker.msfc.nasa.gov
CXC Coordinator		
Belinda Wilkes	CXC Director's Office	belinda@head.cfa.harvard.edu

CXC 2011 Press Releases

Megan Watzke

Date	PI	Objects	Title
10 January	Amy Reines (University of Virginia)	Henize 2-10	Surprise: Dwarf Galaxy Harbors Supermassive Black Hole
12 January	Joey Neilsen (Harvard)	GRS 1915+105	Taking the Pulse of a Black Hole System
23 February	Dany Page (National Autonomous University, Mexico)	Cas A	NASA's *Chandra* Finds Superfluid in Neutron Star's Core
29 March		Einstein Fellows	2011 Einstein Fellows Chosen
07 April	Andrew Levan (University of Warwick)	GRB 110328A	NASA Telescopes Join Forces to Observe Unprecedented Explosion
26 April	Fangjun Lu (Chinese Academy of Sciences)	Tycho SNR	NASA's *Chandra* Finds Evidence on Origin of Supernovas
11 May	Martin Weisskopf/ Allyn Tennant (MSFC)	Crab Nebula	NASA's *Fermi* Spots 'Superflares' in the Crab Nebula
24 May	Leisa Townsley (Penn State)	Carina Nebula	Nearby Supernova Factory Ramps Up
15 June	Ezequiel Treister (University of Hawaii)	CDFS	NASA's *Chandra* Finds Massive Black Holes Common in Early Universe
26 July	Ka-Wah Wong (University of Alabama)	NGC 3115	NASA's *Chandra* Observatory Images Gas Flowing Toward Black Hole
31 August	Pepi Fabbiano (CfA)	NGC 3393	NASA's *Chandra* Finds Nearest Pair of Supermassive Black Holes
13 September	Sebastian Schroeter (University of Hamburg)	CoRoT-2	Star Blasts Planet with X-rays
17 November	Jerome Orosz (San Diego State University) and Lijun Gou (CfA)	Cygnus X-1	NASA's *Chandra* Adds to Black Hole Birth Announcement

STOP for Science!

Kim Arcand and Pat Slane

Young students are often natural scientists. They love to poke and prod, and they live to compare and contrast. What is the fastest animal? Where is the tallest mountain on Earth (or in the Solar System)? Where do the colors in a rainbow come from? And why do baseball players choke up on their bats?

Educators work hard to harness this energy and enthusiasm in the classroom, but particularly at an early age, exposure to science outside the formal classroom is crucial to help expand science awareness and hone science skills. Developed under a grant from *Chandra* EPO with the CXC's Pat Slane, "STOP for Science!" (STOP) is proving to be a simple but effective program that raises questions about science topics in such a way as to capture student interest.

STOP consists of a series of five posters designed to engage any K–6 student in science through relatable and recognizable applications to the world in which we live. The posters can be placed anywhere on school grounds—from hallways to cafeterias—so that the program is not seen as only something for "science" students. The ultimate goal of STOP is to generate school-wide interest about science that can be sustained as the STOP displays are changed throughout the year.

Accompanying each poster is a series of question sheets of increasing difficulty levels that students answer and submit at a designated location (collection box, office, etc.). Random prize drawings can be used to to recognize or celebrate student participation. Although the focus is building-wide, content can be linked to classrooms through use of accompanying teacher/facilitator resource guides.

The following five topics are currently included in the STOP program:

* How Tall is Tall? asks, "What is the tallest mountain on Earth?"
* "When Stars Go Boom!" introduces several key ideas about stars, and focuses in particular on the supernova explosions that mark the ends of the lives of the most massive stars.
* "Choke Up on That Bat!" explores the science behind this technique by introducing the concepts of inertia, force, and torque, though in somewhat more conceptual terminology.
* "That's Fast!" introduces the basic definition of speed, giving simple examples in units that the students can relate to.
* "Somewhere Over The Rainbow" introduces key ideas about light—and sunlight in particular—to explain its behavior when it travels through a raindrop, and how this results in the formation of rainbows.

If you would like to help establish this program at a school near you, please visit the web site and request a copy of the materials at *http://chandra.si.edu/edu/stop/* . If you are interested in helping develop the next generation of STOP materials, please contact cxc-pub@cfa.harvard.edu.

Year of the Solar System

Kim Arcand

The From Earth to the Solar System (FETTSS) is a project created by the *Chandra* EPO group, in collaboration with NASA's Astrobiology Institute, as part of NASA's Year of the Solar System that runs through 2012. Building on the success of the *Chandra* EPO's From Earth to the Universe project, FETTSS places images from across the Solar System in public venues such as parks, libraries and other free-access public venues.

The goal of FETTSS is to show the breadth of NASA science—from heliophysics to planetary science, and, of course, multiwavelength astrophysics. The core of FETTSS is an online repository that encourages replication of exhibits suitable for local adaptation around

Fig. 1. FETTSS visits Washington, D.C. from June–July, 2011. Photo Credit: NASA/CXC/SAO/J.DePasquale

the world, as well as a NASA-funded traveling exhibit visiting over a dozen US locations from 2011–2012. Over 70 locations worldwide—from cafés in New Zealand to malls in Canada—have hosted or have signed up to host a FETTSS event using the online repository. For more information on this *Chandra*-led project, visit *http://fettss.arc.nasa.gov/*

2011 X-ray Astronomy School

Aneta Siemiginowska

The *Chandra* X-ray Center hosted the 6th International X-ray Astronomy School at the Harvard-Smithsonian Center for Astrophysics in Cambridge, MA on August 1–5, 2011. The 2011 X-ray Astronomy School, organized jointly by HEASARC at NASA Goddard Space Flight Center and the *Chandra* X-ray Center, was designed to introduce graduate students and recent postdocs to the intricacies of X-ray astronomy. Thirty-one students from the US, Italy, Spain and Canada attended the school.

The lectures delivered by experts in the field emphasized the foundations of X-ray astronomy, physics of X-ray emission processes, instrumentation and characteristics of detectors, and analysis methods towards correct interpretation of the data. The school also included a hands-on component in which students analyzed an X-ray dataset of their choice using the standard software. Students attended lectures in the morning and practice sessions in the afternoon, and worked on a variety of projects during the week. On the last day, each student presented a short summary of their X-ray Astronomy School Project to the other students and scientists at the final Symposium. The school web page contains the program with posted lectures and links to the science projects: *http://cxc.cfa.harvard.edu/xrayschool/*

The book based on the lectures delivered at several past X-ray astronomy schools was published last fall by Cambridge University Press as "Handbook of X-ray Astronomy" edited by Keith Arnaud, Randall Smith and Aneta Siemiginowska. The book has a web page at *http://xrayastronomyhandbook.com* with more information, tables, figures and errata.

The 2011 X-ray Astronomy School was sponsored by NASA, the *Chandra* X-ray Center, and *XMM-Newton*.

Fig. 1 - 2011 X-ray Astronomy School Participants

Listening to X-ray Data

Wanda Diaz Merced, Matt Schnepps, Nancy S. Brickhouse, G. Juan M. Luna and Stephen Brewster

Astronomy is thought of as a *visual* science, but astronomers have long since exceeded the wavelength range of the human eye. We find many ways to represent otherwise invisible data to our senses. If astronomical data can be represented in diverse ways, the audience for which the data are useful becomes more diverse, and our opportunities for conceptualizing the data expand as well.

At Glasgow University we have developed a tool for rendering space physics data non-visually, through sonification. Sonification can open up the space physics data collection to a new community of researchers now excluded from space physics research, including the visually impaired. In addition, the *sound* of many types of astronomical data allows for a richer intuitive understanding of it by everyone.

Sonification can benefit all students and researchers, allowing them to :

- analyze complex or rapidly/temporally changing data.
- explore large datasets (multi-dimensional datasets).
- intuitively explore datasets in the frequency domain.
- identify new phenomena that current display techniques miss.
- find hidden correlations and patterns masked in visual displays.
- monitor data while doing something else (background event-finding).

For instance, when searching solar data for bow shock and magnetopause crossings, we expect that distinctive signatures will be especially apparent above the background noise. These boundary signatures appear as characteristic changes in the whole spectrum. Other emissions appear as tones at distinctive frequencies or time-frequency spectra (such as electron plasma oscillations, magnetic noise bursts in the magnetosheath, and whistler mode emissions marking regions of currents).

The xSonify tool sonifies 1-dimensional data from text files and from CDAWeb heliophysics data holdings. xSonify is based on Java 1.5 with Java Sound, MIDI, JavaSpeech, WebStart and Web Services technology. xSonify features three different sonification modes (Pitch, Loudness, Rhythm) with various controls (Play, Stop, Loop, Speed, Time point). It includes capabilities for limited pre-processing of input data (Limits, Invert, Logarithm, Averaging). We will further enhance xSonify to handle all 1-dimensional (as well as multi-dimensional) data and add additional features. The source code is openly available at *http://xsonify.sourceforge.net* under the NASA Open Source Agreement (NOSA).

The non-visual representation of data (sonification), made possible through this tool began with NASA support, starting from the Space Physics Data Faciliy (SPDF) requirement to improve access to heliophysics data. This project will also meet the goals of contributing to the development of the science, technology, engineering, and mathematics (STEM) workforce (especially in under-served and under-represented communities) [NASA Education Outcome ED-1] and attract students to STEM disciplines [NASA Education Outcome ED-2].

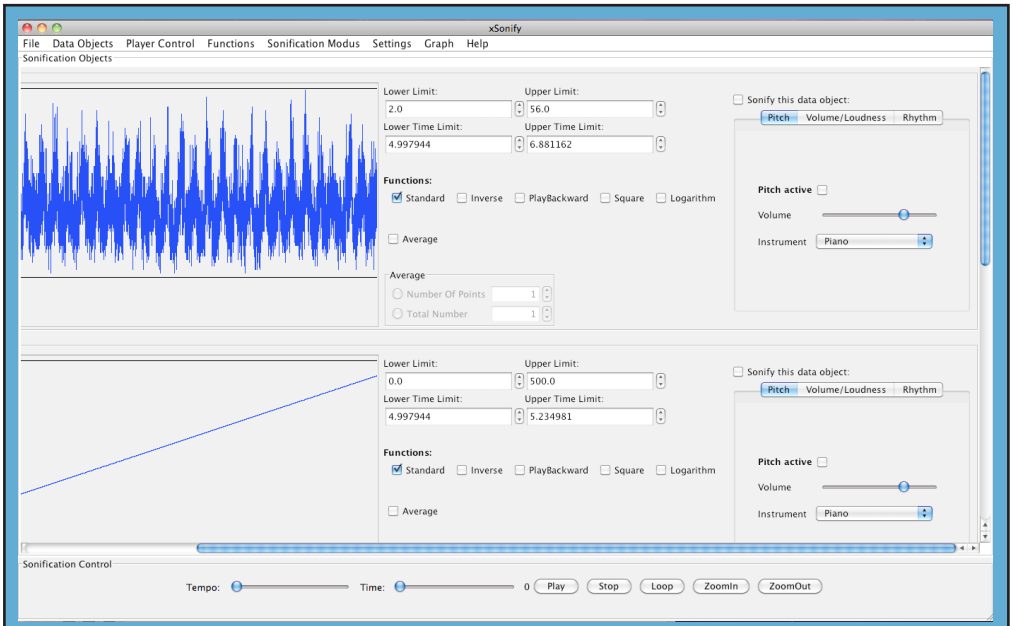

Fig. 1 - The xSonify user interface. Any 1-D data set (e.g., timeseries data, or a spectrum) can be imported into the application. The software will then sonify the data, converting the visible amplitudes (upper left), into auditory information that can be heard, augmenting the visual analysis of the data.

Sonified X-ray Data

EX Hydrae is a southern variable star classified as an eclipsing intermediate polar-type cataclysmic variable (CV) of the DQ Her type. As a binary with an orbital period of 98 minutes, EX Hya belongs to a small group of intermediate polars with ultrashort periods. The observed

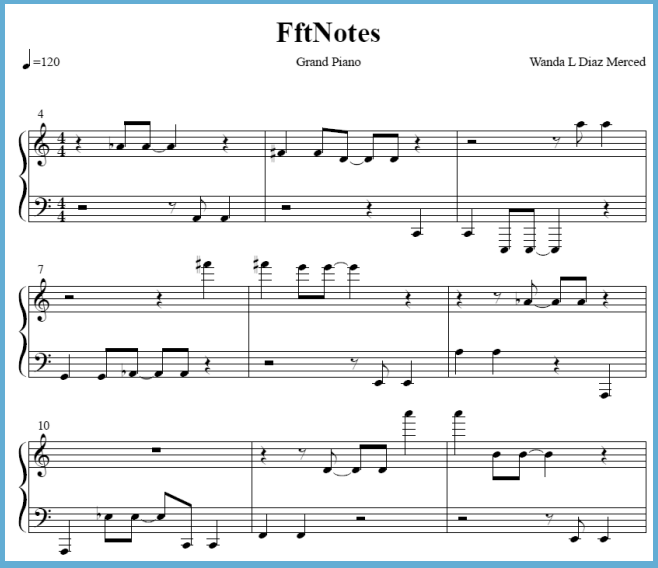

Fig. 2 - First page of a 29 page musical score corresponding to the sonification of the FFT of the *Chandra* X-ray lightcurve of EX-Hya.

67-minute oscillation is believed to be the spin period of the white dwarf component. A long (~500 ks) *Chandra* observation of EX Hya was obtained with HETG and ACIS-S. We sonified the EX Hydra X-ray light curve in pitch mode, normalized to a musical scale, to analyze its frequency content. Temporal fluctuation information is portrayed as simultaneously sounded clusters of pitches. Phase, frequency and time variations as a function of pitch can be grouped and then extracted from the data. Persistent or intermittent features in the data may map to interesting physical parameters of the EX Hya system. Given the human ability to transform the disturbance reaching our ears from the space domain to the frequency domain, this step may be compared to decomposing the data into different simple modes of oscillation.

We listened to the FFT data, binned into segments of 10 min each. The frequency information was represented as musical notes readily familiar to the ear, and the spin period is easily recovered. A period search performed by extracting the harmonics showed several statistically significant periods in the range between 250 and 800 sec.

Perception Experiment

We recently completed perception experiments to investigate the effectiveness of sonification together with visual display for compare event detection in the data as compared to visual display only. A second aim of these experiments was to investigate whether sonification enhances data analysis. These rigorous laboratory experiments on attention control, and human-computer interaction (HCI), will help identify how combining sonification with visualization can enhance scientific data analysis. If new efficiencies or new capabilities are identified, our study seeks to understand how to build on these through training.

The perception experiments include empirical measurement of performance. Here, double-peaked radio-frequency spectra of water maser emission observed in the corners of active galactic nuclei were simulated by a pair of gaussians displayed on the screen, over which random noise was superimposed. Participants were presented simulated spectra and asked to identify the presence of a "signal" obscured by noise, at varying signal-to-noise ratios. Test volunteers experience astronomy data via audio cues, visual cues, both together, and also both cues with a sweep line. The volunteers responded to the cues using the keyboard, and their threshold for detection was estimated using an algorithm called QUEST (Quick Unbiased and Efficient Statistical Tree). We hope our results will bring a more diverse community into data analysis and will open up a multimodal approach to scientific data.

Acknowledgments

This work has been supported by the Smithsonian Women's Committee, the George E. Burch Foundation Fellowship at the Smithsonian, and the Laboratory for Visual Learning at the Science Education Department at the Harvard-Smithsonian Center for Astrophysics .

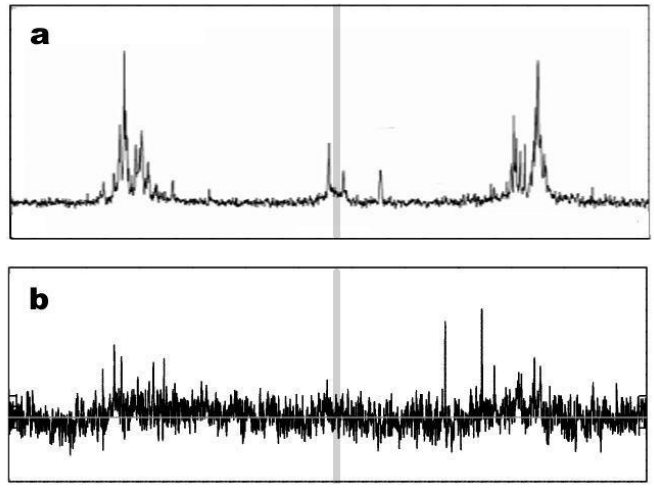

Fig. 3 - Our experiments simulated the double-peaked H_2O emission profiles from active galactic nuclei, here from (a) NGC 3393 and (b) NGC 591. A double gaussian was used to simulate the emission peaks, and random noise was added. The experiments measured the signal-to-noise threshold at which participants were able to reliably detect the "signal" in the presence of noise. The experiment compared response sensitivity in visual presentations, auditory presentations, and combined visual and auditory presentations to gauge the efficacy of sonification for promoting detection.